Journal of Theoretical Biology 256 (2009) 126–141

Contents lists available at ScienceDirect

Journal of Theoretical Biology

journal homepage: www.elsevier.com/locate/yjtbi

The role of low avidity T cells in the protection against type 1 diabetes: A modeling investigation

Anmar Khadra [a,*], Pere Santamaria [b,1], Leah Edelstein-Keshet [a,2]

[a] Department of Mathematics, University of British Columbia, Vancouver, BC, Canada V6T 1Z2
[b] Department of Microbiology and Infectious Diseases, University of Calgary, Calgary, AB, Canada T2N 4N1

ARTICLE INFO

Article history:
Received 22 May 2008
Received in revised form
10 September 2008
Accepted 18 September 2008
Available online 6 October 2008

Keywords:
Diabetes
T cell avidity
Antigen-presenting cell (APC)
β Cell
Modeling

ABSTRACT

Cytotoxic T lymphocytes (CTLs) play a dominant role in the pathogenesis of autoimmune diabetes, commonly denoted Type 1 Diabetes (T1D). These CTLs (notably $CD8^+$ T cells) recognize and kill insulin-secreting pancreatic β cells, reducing their number by ~90%. The resulting reduction of insulin secretion causes the defective regulation of glucose metabolism, leading to the characteristic symptoms of diabetes. Recognition of β cells as targets by CTLs depends on the interactions between MHC-peptide complexes on the surface of β cells and receptors (TCRs) on T cells. Those CTLs with high affinity TCRs (also called high avidity T cells) cause most of the harm, while those with low affinity TCRs (also called low avidity T cells) play a more mysterious role. Recent experimental evidence suggests that low avidity T cells accumulate as memory T cells during the disease and may be protective in NOD mice (a strain prone to developing T1D), delaying disease progression. It has been hypothesized that such low avidity T cells afford disease protection either by crowding the islets of Langerhans, where β cells reside, or by killing antigen presenting cells (APCs).

In this paper, we explore the hypothesized mechanisms for this protective effect in the context of a series of models for (1) the interactions of low and high avidity T cells, (2) the effect of APCs and (3) the feedback from β cell killing to autoantigen-induced T cell proliferation. We analyze properties of these models, noting consistency of predictions with observed behaviour. We then use the models to examine the influence of various treatment strategies on the progression of the disease. The model reveals that progressive accumulation of memory low avidity autoreactive T cells during disease progression makes treatments aimed at expanding these protective T cell types more effective close to, or at the onset of clinical disease. It also provides evidence for the hypothesis that low avidity T cells kill APCs (rather than the alternate hypothesis that they crowd the islets).

1. Introduction

It has been demonstrated that $CD8^+$ T cells play a crucial role in the pathogenesis of Type 1 Diabetes (T1D) (Han et al., 2005a). Such cytotoxic T lymphocytes (CTLs) destroy around 90% of β cells in the pancreas, leading to the abolishment of insulin production and elevation of blood glucose. There are several stages in the disease progression that ultimately lead to autoimmune attack by CTLs. Here we are mainly concerned with the final stage when $CD8^+$ and $CD4^+$ T cells target and kill β cells.

Naive T cells mature in the thymus and migrate to the lymph nodes where they encounter antigen presenting cells (APCs). Receptors on the surface of T cells (TCRs) then interact with APC surface complexes. These peptide-MHC complexes (p-MHC) consist of a 9-amino acid peptide "antigen" held in the cleft of a major histocompatibility complex (MHC) molecule. Interactions of appropriate strength, duration and frequency between TCRs and p-MHC complexes subsequently lead to T cell activation and proliferation. Some of the progeny become terminally differentiated CTLs and some become memory cells (Sallusto and Lanzavecchia, 2001).

T cells have thousands of identical receptors on their surfaces (Viola and Lanzavecchia, 1996). Binding and unbinding a given TCR to a given p-MHC is reversible, with specific association and dissociation rates $k_{on}(\mu M^{-1}s^{-1})$ and k_{off} (s^{-1}), respectively. The ratio $1/K_D$, where $K_D = k_{off}/k_{on}$ (μM), describes the relative affinity of these receptors to a given peptide. It is often easiest to measure a population average of such interactions, and the term "avidity" is used to describe the average strength of association of a T cell population as a whole.

* Corresponding author: Tel.: +1 604 822 6754; fax: +1 604 822 6074.
E-mail addresses: akhadra@iam.ubc.ca, anmar.khadra@gmail.com (A. Khadra), keshet@math.ubc.ca (L. Edelstein-Keshet).
[1] Tel.: +1 403 220 8735; fax: +1 403 270 8520.
[2] Tel.: +1 604 822 5889; fax: +1 604 822 6074.

0022-5193/$ - see front matter Crown Copyright © 2008 Published by Elsevier Ltd. All rights reserved.
doi:10.1016/j.jtbi.2008.09.019

Research on T1D has been greatly aided by studies of an animal model, the nonobese diabetic (NOD) mouse. These mice are prone to a form of autoimmune diabetes that closely resembles human T1D. The causes of T1D are still obscure, but it has been proposed that defective clearance of dead β cells (after normal developmental wave of apoptosis, or after infection or injury) can set the stage (O'Brien et al., 2002a, b; Marée et al., 2005, 2006a). Priming of $CD8^+$ T cells occurs in the pancreatic lymph nodes, where β cell derived autoantigen is presented on APCs. Extensive work with artificially constructed peptide libraries (Anderson et al., 1999; Han et al., 2005a; Lieberman et al., 2003, 2004) led to the discovery and identification of a dominant autoantigen in NOD mice, a fragment consisting of amino acids 206-214 of islet specific glucose-6-phosphatase catalytic subunit-related protein ($IGRP_{206-214}$, henceforth abbreviated IGRP in this paper). The function of this protein is still unclear, but it is suspected that its native location (embedded in the endoplasmic reticulum of β cells) may be associated with its diabetogenic potential.

Recent work (Han et al., 2005b) has experimentally identified three arbitrary levels of T cell avidity for $IGRP_{206-214}$/MHC: low, intermediate, and high. Han et al. (2005b) described three clonotypes that fall within each of these three different levels of avidity (denoted 17.6, 17.4 and 17.5, respectively). High and intermediate avidity T cells are the most pathogenic and damaging to β cells, whereas the effect of low avidity T cells remains obscure. In the progression of T1D, high to intermediate avidity T cells eventually come to dominate the population. The process leading to this outcome, called avidity maturation, is believed to result from competitive survival of T cell clones with high affinity TCRs at the expense of their low avidity counterparts (Han et al., 2005b; Marée et al., 2006b).

Recent experimental evidence from the Santamaria Laboratory suggests that low avidity T cells play a protective role in NOD mice (Tsai et al., 2008). In particular, it has been shown experimentally that treatments aimed at expanding the pool of low avidity T cells are effective in treating diabetic NOD mice. FACS analysis has revealed that this pool of low avidity T cells contains a significantly expanded sub-pool of memory cells (Han et al., 2005b), whereas the high and intermediate avidity T cell pools are primarily composed of naive and effector cells.

One of our goals is to explore how low avidity memory T cells might obstruct the progression of the disease (see Fig. 1). Here we examine the following two hypotheses suggested by Tsai et al. (2008):

(I) The population of low avidity T cells expand with treatment and infiltrate the islets. Then they crowd these islets and interfere with the ability of other clones of autoreactive T cells to kill β cells.

(II) Memory cells that accumulate solely in the low avidity T cell pool, kill APCs presenting $IGRP_{206-214}$/MHC complexes on their surface, both *in vitro* and *in vivo*, thereby inhibiting the activation (mediated by APCs) of their high and intermediate avidity counterparts in the lymph nodes.

We discuss alternative scenarios for their protective effect in the Discussion.

Another goal is to assess the relative efficacy of various treatment strategies and to explain why some are ineffective when applied to prediabetic NOD mice, and much more effective at the acute diabetic stage. Our models are related to those of Marée et al. (2006a) and Mahaffy and Edelstein-Keshet (2007) in general, but we focus here on more recent experimental observations.

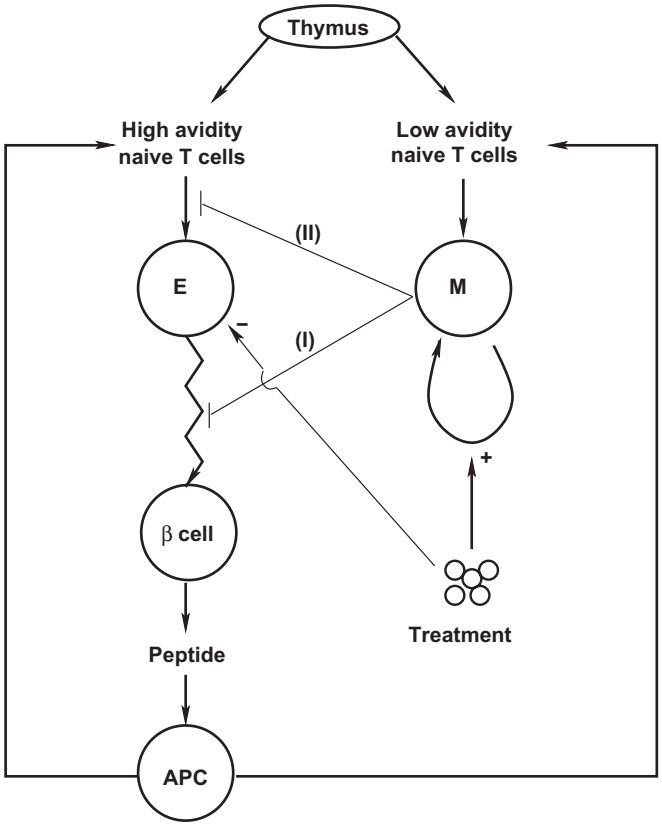

Fig. 1. A scheme showing proposed hypotheses for the effect of low avidity T cells. The thick lines represent confirmed activation and inhibition exerted by the corresponding factors, while thin lines represent hypothetical influences to be investigated by the model. *E* represents high and intermediate avidity T cells that are mostly naive and effector cells, while *M* represents low avidity T cells that are enriched for memory cells. The lines corresponding to hypotheses (I) and (II) are shown.

The paper is organized as follows. In Section 2, we introduce the general model framework and derive its essential features from the underlying biology. In Section 3, we explore a two-variable reduced model for the competition of low and high avidity T cell populations. We later extend this model to include first APCs (Section 4) and then β cells (Section 5). Discussion and physiological significance of these results are given in Section 6.

2. Model framework

A schematic diagram summarizing our model framework is shown in Fig. 1. We consider the following cell types: (a) high avidity T cells (consisting mostly of naive and effector cells with only a small fraction of memory cells for self-renewal); (b) low avidity T cells (enriched for memory cells); (c) β cells and (d) APCs. The population levels of these cells are denoted by E, M, B and A, respectively. We also include the level of autoantigen peptide, P, stemming from dead β cells. Here, various phenotypes within low/high avidity T cell clones are lumped together.

The following assumptions are based on experimental observations (Han et al., 2005a, b; Marée et al., 2006b).

1. Low avidity T cells do not kill β cells, but they compete with other T cells. Since this pool is enriched for memory cells, they are long-lived (low decay rate) and proliferate rapidly in the presence of high level of autoantigen. Due to their low avidity, they require more peptide for activation.

2. High avidity T cells are largely effector cells (or their naive precursors) that kill β cells. They are short-lived (high decay rate). A small fraction of memory cells in this pool allows for self-renewal. Due to their high avidity, these cells can become activated at lower levels of peptide.
3. Activation of high and low avidity T cells depends on the amount of peptide present. Increasing the peptide level leads to increased activation up to some saturation level.
4. According to hypothesis (I), high avidity T cells kill β cells, while low avidity T cells crowd the islets and inhibit β cell killing.
5. According to hypothesis (II), low avidity T cells induce APC death by apoptosis.
6. The rate of change of β cells is slow relative to other rates while the rate of change of autoantigen is fast. This assumption can be restated as follows: β cells initially compensate for T cell mediated killing by regeneration, so that the β cell population is not seen to change rapidly. However, the peptide produced from dead β cells accumulates rapidly, possibly due to defects in the clearance of dead cells (see, e.g., Marée et al., 2005).

The equations for low avidity memory cells (M), high avidity effector cells (E), APCs, (A), β cells (B), and peptide autoantigen (P) are of the general form:

$$\frac{dM}{dt} = \sigma_m + M\mathscr{F}(M,E,A,P) \tag{1}$$

$$\frac{dE}{dt} = \sigma_e + E\mathscr{G}(M,E,A,P) \tag{2}$$

$$\frac{dA}{dt} = \sigma_a - AQ_1(M) \tag{3}$$

$$\frac{dB}{dt} = B[Q_2(B) - K(M,E,B)] \tag{4}$$

$$\frac{dP}{dt} = BK(M,E,B) - \delta_P P \tag{5}$$

Here σ_m and σ_e are the thymus input for both types of T cells, σ_a is the bone-marrow input for APCs. $\mathscr{F}$ and $\mathscr{G}$ represent the net population growth rates (of M and E, respectively) resulting from combined rates of activation, proliferation, turnover and competition. The function Q_1 represents normal turnover and (hypothetical) deletion of APCs by low avidity T cells (if any), while the function Q_2 represents β cell replication, neogenesis and turnover. The killing of β cells by high avidity effector T cells and the inhibition of this killing process exerted by low avidity T cells are portrayed by the function K. Finally, the term $\delta_P P$ denotes peptide clearance. Based on Fig. 1 and the assumptions listed above, the following inequalities must hold:

(i) APCs are required for T cell activation. Therefore

$$\frac{\partial\mathscr{F}}{\partial A}, \quad \frac{\partial\mathscr{G}}{\partial A} \geqslant 0$$

(ii) Inter and intra specific competition between high and low avidity T cells require that

$$\frac{\partial\mathscr{F}}{\partial M}, \quad \frac{\partial\mathscr{G}}{\partial M}, \quad \frac{\partial\mathscr{F}}{\partial E}, \quad \frac{\partial\mathscr{G}}{\partial E} \leqslant 0$$

(iii) Killing of APCs by low avidity T cells and killing of β cells by high avidity T cells imply

$$\frac{dQ_1}{dM}, \quad \frac{\partial K}{\partial E} \geqslant 0$$

(iv) Normal β cell homeostasis implies that β cell growth is "density dependent" and decreases as β cell density or mass increases. Hence

$$\frac{dQ_2}{dB} \leqslant 0$$

(v) According to hypothesis (I), β cell killing by high avidity T cells is inhibited by low avidity T cells. It follows that

$$\frac{\partial K}{\partial M} \leqslant 0$$

The general model (1)–(5) together with the latter inequalities will form the framework for formulating simpler, more specific, models in the following sections.

3. Two-dimensional model for T cell competition

3.1. Model reduction

It is instructive to consider a two-variable submodel for T cell competition with the following simplifications. First, we use the fact that the dynamics of β cells is very slow on the time scale of T cell activation, due to homeostatic mechanisms that regulate the β cell population. In that case, $B \approx$ constant. However, as β cells are killed, peptide rapidly accumulates due to clearance defects, indicating fast peptide dynamics (Assumption 6); this justifies a quasi-steady state (QSS) approximation for the peptide, given by

$$P \approx RE$$

for some constant $R>0$. For simplicity, we also assume that

7. The total number of APCs in the lymph nodes is roughly constant.
8. Thymus input is relatively small compared to other dynamics during the heightened level of T cell populations.

These simplifications lead to a reduced two-variable model for E and M,

$$\frac{dM}{dt} = MF(M,E) \tag{6}$$

$$\frac{dE}{dt} = EG(M,E) \tag{7}$$

The role of the peptide has been subsumed in the effector cell population. It follows that, with this reduction, $\partial G/\partial E$ and $\partial F/\partial E$ could be either positive or negative, since the effector cell population leads (indirectly) to activation as well as to competition in both equations.

In these equations, we have omitted the small input of naive T cells from the thymus, σ_m and σ_e, by Assumption 8. This simplification makes the model considerably more transparent for the purposes of our analysis, without significantly affecting its overall qualitative behaviour. (The simplification essentially subtracts a background population of autoreactive T cells that are found in normal individuals.)

3.2. Model properties

We first proceed to explore properties of this model in an "axiomatic approach" (in the sense of Shochat et al., 2007). First, since not all NOD mice develop diabetes, it follows that system (6)–(7) should possess at least two stable steady states:

- A "healthy" state at $\mathbf{S}_1 = (0,0)$. This state corresponds to nondiabetic NOD mice, or mice that have been treated and recovered from the disease. (It may also represent acutely

diabetic mice that have lost their β cell function, leading to eventual decline in T cell repertoires. Hence the transient dynamics leading to this state are important.)

- A heightened autoimmune "diseased" state $\mathbf{S}_2 = (M_2, E_2)$ (where $E_2 \gg M_2 > 0$, i.e., expansion in the population of both clones of T cells is observed). This state corresponds to acutely diabetic NOD mice. For $\mathbf{S}_2$ to be a steady state, we need $F(\mathbf{S}_2) = G(\mathbf{S}_2) = 0$.

The existence of such stable steady states is a minimal prerequisite for any model that describes both healthy and autoimmune compromised situations. Stability of these steady states implies that

$$F_M \equiv \left.\frac{\partial F}{\partial M}\right|_{SS} < 0, \quad G_M \equiv \left.\frac{\partial G}{\partial M}\right|_{SS} < 0 \tag{8}$$

where partial derivatives are evaluated at the given steady state. In Appendix A, we show that $\mathbf{S}_2$ is stable if and only if

$$D_m|_{\mathbf{S}_2} > D_e|_{\mathbf{S}_2} \quad \text{and} \quad D_e|_{\mathbf{S}_2} < \frac{M_2}{E_2}\left|\frac{F_M(\mathbf{S}_2)}{G_M(\mathbf{S}_2)}\right| \tag{9}$$

where D_m is the slope of the tangent line to the nullcline $F(M,E) = 0$ and D_e is the slope of the tangent line to the nullcline $G(M,E) = 0$.

System (6) and (7) can also have other steady states in which either low avidity T cells are absent, $\mathbf{U}_1 = (0, \mathscr{E}_1)$, or high avidity T cells are absent, $\mathbf{U}_2 = (\mathscr{M}_2, 0)$ (where $\mathscr{E}_1, \mathscr{M}_2 > 0$). Some of these can be stable, unstable or saddle points. In Appendix A, it is shown that $\mathbf{U}_1$ and $\mathbf{U}_2$ are stable whenever $F(\mathbf{U}_1), G_E(\mathbf{U}_1) < 0$, and $G(\mathbf{U}_2) < 0$, respectively, and saddle or unstable otherwise. By comments following Eq. (7), G_E can have either sign.

Cyclic fluctuations of T cell populations have been found to be directly correlated to pathogenesis of T1D in NOD mice (Trudeau et al., 2003). The possible significance of cyclic behaviour in relapse and remission of diabetes has been pointed out recently by von Herrath et al. (2007). Cyclic dynamics were explored in a previous modeling work (Mahaffy and Edelstein-Keshet, 2007). Such cycles can be understood in the context of a Hopf bifurcation, a hallmark of the birth of a limit cycle in the corresponding model. In Appendix A, we derive the necessary and sufficient conditions for the existence of a Hopf bifurcation point $\mathbf{H} = (h_1, h_2)$, satisfying $F(\mathbf{H}) = 0$ and $G(\mathbf{H}) = 0$. These conditions are

$$D_m|_{\mathbf{H}} > D_e|_{\mathbf{H}} \quad \text{and} \quad D_y|_{\mathbf{H}} = \frac{h_1}{h_2}\left|\frac{F_M}{G_M}\right| \tag{10}$$

Generic features of the model so far allow us to link properties of the functions F and G to steady state properties. However, the detailed dynamics are much more important. Diabetes can occur when a transiently high level of effector cells causes significant β cell killing before eventually decaying to a low level. Here the system eventually evolves to the autoimmune-free state (denoted by $\mathbf{S}_1$), but the consequences are dire. To predict whether this happens or not, it is essential to understand the full dynamics of the model. To do so, we must make more detailed assumptions about the functions F and G, as done in the next section.

3.3. Explicit form of the two-variable model

For further analysis, we adopt the following forms for the T cell growth rates, $\tilde{F}$ and $\tilde{G}$:

$$\begin{aligned}\tilde{F}(M,E,P) &= \alpha_m \tilde{f}_m(P) - \delta_m - \varepsilon(M+E)\\ \tilde{G}(M,E,P) &= \alpha_e \tilde{f}_e(P) - \delta_e - \varepsilon(M+E)\end{aligned} \tag{11}$$

with $P \approx RE$ (from the peptide QSS). Terms in formulae (11) denote (1) peptide-dependent T cell proliferation after activation (maximal rate α_i); (2) T cell death rate (δ_i); and (3) inter and intra specific competition of T cells ($\varepsilon(M+E)$). (As in De Boer and Perelson, 1994; Marée et al., 2006b, we have assumed the same level of competition ε for all T cells to avoid competitive exclusion.)

For peptide-dependent rates of activation, we take

$$\tilde{f}_m(P) = \frac{P^n}{K_m^n + P^n} \quad \text{and} \quad \tilde{f}_e(P) = \frac{P^n}{K_e^n + P^n}$$

with $n \geqslant 2$. Here K_m is the level of peptide that leads to activation of 50% of naive low avidity T cells (at the rate of α_m), and similarly for K_e. As there is no simple way of calibrating the absolute amounts of autoantigen peptide *in vivo*, we rescale these functions, by substituting $P \approx RE$ and defining $k_i = K_i/R$, for $i = m, e$. We thus obtain

$$f_m(E) = \frac{E^n}{k_m^n + E^n} \quad \text{and} \quad f_e(E) = \frac{E^n}{k_e^n + E^n}$$

Now k_i represents the effective number of high avidity T cells that lead to activation of half of the naive i-type T cells. Observe that varying the parameter R has an influence on the two threshold parameters k_m and k_e. In other words, in this model, decreasing (increasing) the production of endogenous peptide per effector cell is effectively the same as decreasing (increasing) the avidity of both populations of T cells. The model equations, based on these choices, is then

$$\begin{aligned}\frac{dM}{dt} &= \alpha_m\left(\frac{E^n}{k_m^n + E^n}\right)M - \delta_m M - \varepsilon M(M+E)\\ &= MF(M,E)\end{aligned} \tag{12}$$

$$\begin{aligned}\frac{dE}{dt} &= \alpha_e\left(\frac{E^n}{k_e^n + E^n}\right)E - \delta_e E - \varepsilon E(M+E)\\ &= EG(M,E)\end{aligned} \tag{13}$$

Furthermore, according to Assumptions 1–3, it follows that

$$\delta_e > \delta_m, \quad \alpha_m > \alpha_e, \quad k_m > k_e \tag{14}$$

The first inequality stems from the fact that the variable E represents mostly effector T cells, and very few memory cells. The average life expectancy of this population is thus much shorter than that of M (which mainly consists of long-lived memory cells). The makeup of the two populations also implies that M has a much higher self-renewal potential than E, accounting for the second inequality. The third inequality stems from the fact that high avidity T cells are more acutely sensitive to peptide. Typical graphs of the activation rates $g_i(E) \equiv \alpha_i f_i(E)$, for $i = m, e$, satisfying inequalities (14), are shown in Fig. 2(b).

In this basic model, only competition between cells of type M and E is considered. We use this simplest variant to explore features of this competition before attempting to investigate hypotheses I and II about subtler roles of low avidity T cells.

3.4. Phase plane analysis

Eqs. (12) and (13) can be fully analyzed with phase-plane methods. As shown in Fig. 3, steady states are located at intersections of nullclines, given by

(I) *M-nullclines*:

$$M = 0 \quad \text{and} \quad M = \frac{\alpha_m}{\varepsilon}f_m(E) - \frac{\delta_m}{\varepsilon} - E \equiv \widetilde{g}_m(E)$$

(II) *E-Nullclines*:

$$E = 0 \quad \text{and} \quad M = \frac{\alpha_e}{\varepsilon}f_e(E) - \frac{\delta_e}{\varepsilon} - E \equiv \widetilde{g}_e(E)$$

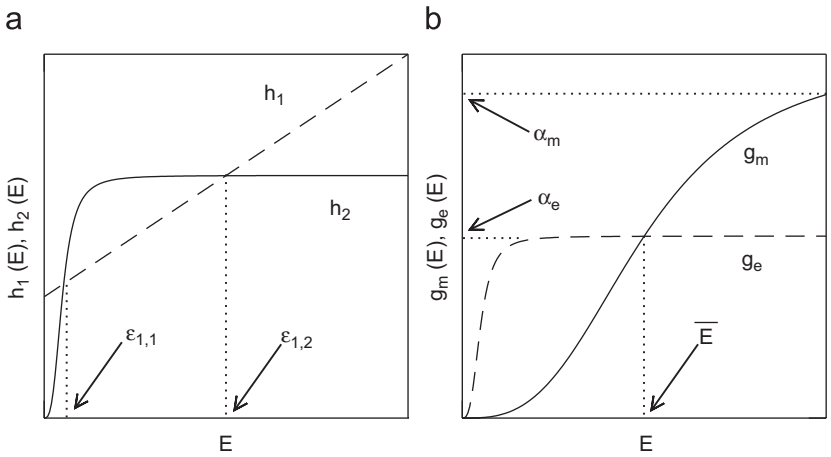

Fig. 2. Typical graphs of the functions obtained by solving for the equilibrium points of system (1) and (2). (a) Graphs of the functions $h_1(E)$ and $h_2(E)$. (b) Graphs of the functions $g_m(E)$ and $g_e(E)$.

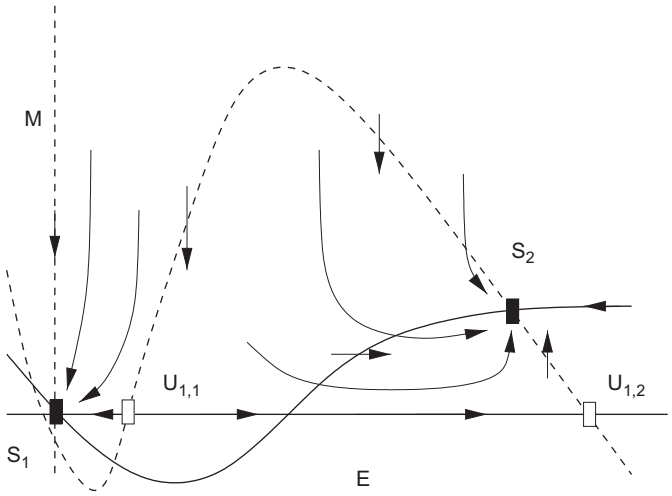

Fig. 3. Behaviour of the reduced model (12) and (13) governed by the nullclines for M (thick solid lines) and E (dashed lines). Points labeled with solid rectangles ($\mathbf{S}_1$ and $\mathbf{S}_2$) are the healthy and the autoimmune "diseased" states, respectively (both stable). Other steady states labeled with open rectangles are unstable, but their number, location, and types of stability help to carve out the basins of attraction of $\mathbf{S}_1$ and $\mathbf{S}_2$. Parameter variations that affect the shapes and heights of the nullclines (see Fig. 4) will change the locations and stability of the steady states, and thus the essential behaviour of the model. Thin lines represent typical trajectories that evolve towards the healthy or diseased states.

We are primarily interested in the steady states $\mathbf{S}_1$ and $\mathbf{S}_2$, but others can influence basins of attraction, and thus be of relevance to the dynamics.

- The intersection of $M=0$ and $E=0$ nullclines generates the steady state $\mathbf{S}_1=(0,0)$ at which both T cell populations are at their normal "healthy" baseline level (previously denoted "healthy state").
- The autoimmune "diseased" state, $\mathbf{S}_2$, is at the intersection of $M=\widetilde{g}_m(E)$ and $M=\widetilde{g}_e(E)$, at which both M and E are elevated. We consider this in greater detail below.
- The nullclines $M=0$ and $M=\widetilde{g}_e(E)$ can intersect each other at up to two points, depending on the values of ε, α_e and δ_e. When $M=0$ and $M=\widetilde{g}_e(E)$, $g_e(E)=0$, i.e., $h_1(E)\equiv\delta_e+\varepsilon E=\alpha_e f_e(E)\equiv h_2(E)$. Fig. 2(a) shows that positive steady states can occur in this case. We may either have no equilibrium points, one equilibrium point ($\mathbf{U}_1=(0,\mathscr{E}_1)$) or two ($\mathbf{U}_{1,1}=(0,\mathscr{E}_{1,1})$ and $\mathbf{U}_{1,2}=(0,\mathscr{E}_{1,2})$) depending on parameter values.
- At the intersection of $E=0$ and $M=\widetilde{g}_m(E)$, there is an unstable and physiologically irrelevant steady state at $\mathbf{U}_2=(-\delta_m/\varepsilon,0)$.

Existence of the autoimmune state $\mathbf{S}_2$ (with $M,E>0$) requires that

$$\alpha_m f_m(E)-\delta_m=\alpha_e f_e(E)-\delta_e \Longrightarrow g_m(E)-g_e(E)=\delta_m-\delta_e<0 \quad (15)$$

Inequality (15) follows from the fact that $\delta_m<\delta_e$, and implies that $g_m(E)-g_e(E)$ must be negative. In Appendix A, we disclose conditions on the parameters that lead to two, one or no such intersections. As far as treatment strategies are concerned, manipulations of the system that increase effector cell turnover rate δ_e, or change the difference in the activation rates $g_m(E)-g_e(E)$, can lead to the disappearance of the autoimmune state.

One basic configuration of the phase plane for system (12) and (13) is shown in Fig. 3. For this basic case, there are four biologically relevant steady states, $\mathbf{S}_1$, $\mathbf{S}_2$, $\mathbf{U}_{1,1}$, and $\mathbf{U}_{1,2}$, the first two of which are stable. From the trajectories on this sketch (thin lines with arrows), we see that the initial values of M and E will determine whether the system evolves towards health ($\mathbf{S}_1$) or disease ($\mathbf{S}_2$). This raises the question of whether treatment strategies can be devised to bring the state of the system, initially at or close to $\mathbf{S}_2$, to a new state close enough to $\mathbf{S}_1$ that it would evolve to the healthy state. In practice, for a range of biologically relevant parameter values, we find that the basin of attraction of $\mathbf{S}_1$ is a very narrow strip along the M axis left of $\mathbf{U}_{1,1}$ (see, for example, Fig. 4(a)–(c)), making this possibility unlikely.

3.5. Estimating parameters and scaling the model

In order to be more accurate about the qualitative behaviour described in Fig. 3, we must estimate ranges of the relevant parameters. Our basic strategy in estimating values of the parameters is briefly highlighted here, with detailed calculations shown in Appendix B.

Detailed kinetic parameters are not available biologically. Some values for turnover rates (δ_m,δ_e), rates of proliferation, etc., have been previously estimated in Marée et al. (2006b) and Mahaffy and Edelstein-Keshet (2007). Where relevant, we assign similar values. The levels of circulating CTLs at the height of autoimmunity, together with known turnover rates of effector and

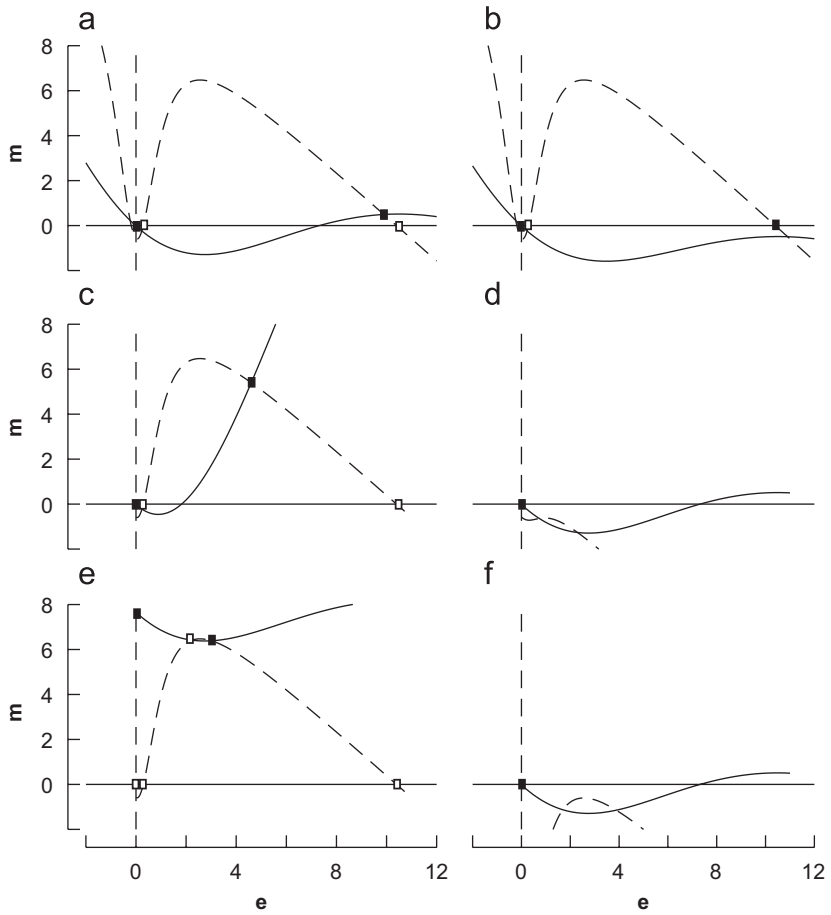

Fig. 4. Six different configurations of the nullclines of system (A.8) and (A.9). Panel (a) is obtained by using the default parameter values listed in Tables 1 and 2 while every other panel is obtained by changing one parameter value at a time. m-Nullclines are plotted in solid lines and e-nullclines are plotted in dashed lines. Stable steady states (healthy and autoimmune states) are highlighted by solid black boxes while saddle points are highlighted by white boxes in each panel. Due to the depletion of the highly avid pool of 17.5 clone, the avidity ratio between m and e declines from high values, as in (b) $k_m/k_e = 11$, to lower values, as in (a) $k_m/k_e = 10$. In the remaining panels, the following parameter values have been used: (c) $\alpha_m = 30$, (d) $\alpha_e = 1$, (e) $r_m = 4$, and (f) $\delta_e = 4$.

memory cells, allow us to estimate the rates of proliferation (α_m, α_e) and competition (ε) (see Appendix B).

We have no direct information about the absolute peptide (or p-MHC) levels for activating T cells, so the parameters k_e and k_m are difficult to determine. However, indirect evidence for relative functional avidity of T cell clones allows us to estimate the ratio k_m/k_e. Based on this fact, it is helpful to consider a substitution $M = k_e m$ and $E = k_e e$ to obtain a scaled version of the model given by system (A.8) and (A.9) in Appendix A. The rescaled model has the advantage of replacing the (unknown) avidity parameters k_m and k_e by their ratio k_m/k_e. A summary of the estimated values of parameters is given in Table 1.

3.6. Analysis of the model

For the default parameter values, given in Tables 1 and 2, it can be shown (using previously derived stability conditions) that $\mathbf{S}_1$ is always stable, $\mathbf{U}_{1,1}$ is always unstable (or a saddle), while $\mathbf{U}_{1,2}$ is stable when it is the only existing autoimmune state (case (a)) and a saddle in the presence of $\mathbf{S}_2$ (case (b)). The stability of $\mathbf{S}_2$, on the other hand, depends on its location along the nullcline $G(m, e) = 0$, as described by conditions (9). But for a large range of physiologically reasonable k_m/k_e values in the range $2 \leqslant k_m/k_e \leqslant 10$, $\mathbf{S}_2$ is stable (see Appendix A for more details). The coexistence of these healthy and autoimmune states is essential if the model is to account for both healthy and diabetic NOD mice.

3.7. Parameter variations and bifurcations

3.7.1. Phase plane configurations

Fig. 4(a)–(i) displays a variety of possible phase plane configurations for parameter values within their biological ranges. Case (a) corresponds to the sketch shown in Fig. 3, while other panels represent cases where only a single parameter has been altered from the default set. In each panel, steady states lie at the intersections of the solid and dashed lines, but only those in the first quadrant $(m, e \geqslant 0)$ are biologically relevant. Steady states are labeled with symbols as in Fig. 3. Note the proximity of $\mathbf{S}_1$ (at (0,0)) to a neighboring unstable state (open rectangle) in Fig. 3(a)–(c). This proximity restricts the basin of attraction of $\mathbf{S}_1$ to a very small region, very close to the origin. Cases in which the origin is the only point of intersection, correspond to eliminating the diseased states ($\mathbf{S}_2$ or $\mathbf{U}_{1,2}$) and represent a desirable treatment outcome.

We begin by investigating the influence of the avidity ratio k_m/k_e by considering the dynamics for two distinct values shown in Fig. 4(a) and (b). In both cases, we observe the coexistence of the healthy state (at (0,0)) and an autoimmune state with sizable population of high avidity T cells (solid rectangles). Changing the value of k_m/k_e can lead to movement and exchange of stability between the two states $\mathbf{U}_{1,2}$ and $\mathbf{S}_2$. For $k_m/k_e \sim 11$ there are no memory cells at the peak of autoimmunity (Fig. 4(b)), while for $k_m/k_e \sim 10$, some small level of such cells persists (state $\mathbf{S}_2$ in Fig. 4(a)).

Table 1
Values of the standard parameters appearing in each model

Symbol	Meaning	Value	Range
M_d, E_d	# of memory, effector cells (disease)	0.5, 10×10^5 cells	$[10^4-10^5]$, 10^6
α_m, α_e	APC-dependent expansion rate of M, E	11, 5.79 day^{-1}	[10–20], [5–10]
$\overline{\alpha}_m$, $\overline{\alpha}_e$	$\approx \alpha_m/A_d$, $\approx \alpha_e/A_d$	2.75, 1.45×10^{-5} $(\text{cell day})^{-1}$	[2.5–5], $[1.25-2.5]\times10^{-5}$
δ_m, δ_e	M, E turnover rates	0.01, 0.03 day^{-1}	
K_m, K_e	Peptide level for $\frac{1}{2}$ max activation of M, E		
$k_m=\frac{K_m}{R}$	Effector level for $\frac{1}{2}$ max activation of M	10^6 cells	$[1-1.4]\times10^6$
$\frac{K_m}{K_e}=\frac{k_m}{k_e}$	Avidity ratio	10	[2–11]
ε	Competition parameter	5.23×10^{-6} $(\text{cell day})^{-1}$	$[5-10]\times10^{-6}$
$\overline{\varepsilon}$	$\approx \varepsilon A_d$	2.092 day^{-1}	[2–4]
δ_a	Turnover rate of APCs	0.3 day^{-1}	[0.24–0.46]
σ_a	Influx of APCs from bone marrow	3×10^5 cell/day	$[3-4]\times10^5$
k_a	Killing rate of APCs	8.5×10^{-6} $(\text{cell day})^{-1}$	$[8-9]\times10^{-6}$
A_d	# of APCs at autoimmune state	4×10^5 cells	
B_h	# of β cells at healthy state	5.8×10^5 cells	$[5-6]\times10^5$
s	β cell renewal rate	662.86 cell/day	[560–1000]
k_B	$\frac{1}{2}$ max renewal rate ofβ cells	9.21×10^3 cells	$[7.5-11]\times10^3$
d	β cell turnover rate	0.001 day^{-1}	[0.001–0.007]
κ	Killing rate of β cells	0.14×10^{-6} $(\text{cell day})^{-1}$	$[0.12-0.15]\times10^{-6}$
μ_0	Per β cell saturation parameter	1.72×10^{-6} cells^{-1}	$[1.67-20]\times10^{-6}$
μ_1	Per memory cell saturation parameter	3.376×10^{-4} cell^{-1}	$[1.1-3.6]\times10^{-4}$
$\overline{R}$	Peptide accumulation rate	2.845×10^{-4} peptide-units/cell^2	$[2.7-3.2]\times10^{-4}$

Table 2
Values of the scaled parameters appearing in each model

Symbol	Value
ε^*	0.523
k_b	0.0159
α_m^*	2.75
κ^*	0.014
α_e^*	1.45
μ_0^*	1
k_a^*	0.85
μ_1^*	33.76
$\overline{\varepsilon}^*$	0.2092
R^*	165
s^*	0.0011

Next, we investigate the effects of changing the proliferation rates, whose default values are in the range of $\alpha_m\approx10$ and $\alpha_e\approx6$ day^{-1}. Increasing the proliferative rate of low avidity T cells to higher values (e.g., to $\alpha_m=30\,\text{day}^{-1}$ as in Fig. 4(c)) shifts (but does not eliminate) the diseased state $\mathbf{S}_2$. Now that state contains much higher levels of memory cells, and somewhat lower levels of effector cells. The overall dynamics is not significantly altered. In contrast, decreasing the proliferative rate of high avidity T cells to $\alpha_e=1\,\text{day}^{-1}$ (Fig. 4(d)) eliminates the diseased state (and any other elevated autoimmune state) altogether. This stems from the feedback exerted by these T cells onto their own and other T cells' activation (via formation of autoantigen, implicit in the reduced model).

We have investigated the effects of changing the turnover rates of the two types of T cells, whose default values are $\delta_m\approx0.01$ and $\delta_e\approx0.3\,\text{day}^{-1}$ (Fig. 4(e) and (f)). There is little room for decreasing the (already low) mortality rate δ_m. However, we may consider possible treatments, wherein memory T cells are artificially expanded in an APC-independent manner. As in Tsai et al. (2008), this could mean injecting "artificial APCs" laden with peptide, that expand the memory cell pool (and kill effector cells, or leave these unaffected). To consider this scenario, we modify the (scaled version of) model Eq. (12) to

$$\frac{dm}{dt}=m\left(\alpha_m\frac{e^n}{(k_m/k_e)^n+e^n}+r_m-\delta_m-\varepsilon^*(m+e)\right)$$

(See Appendix A for the definition of ε^* and note that only M and E were scaled, for convenience, whereas time still carries conventional units.) In Fig. 4(e), we implement this variant with $r_m=4$ (units of day^{-1}), the rate of treatment-induced expansion of memory cells. This can lead to much higher levels of M in both "health" and "disease" (as shown in Fig. 4(e), where several intersections appear in the first quadrant). However, by comparison, increasing the death rate of high avidity T cells to $\delta_e=4\,\text{day}^{-1}$ eliminates all first quadrant intersections including the diseased state (Fig. 4(f)).

The panels of Fig. 5(a)–(f) illustrate the same ideas by showing the time behaviour of both T cell populations (m in dashed, e in solid lines on logarithmic scale) over time (linear scale in days). In each panel, two different initial conditions are shown. In some cases, e.g., panels (a)–(c) and (e), the ultimate result depends on the initial state; some situations evolve towards an elevated level of effector cells ("autoimmunity"), while others resolve to very low values of m and e ("health"). In certain cases, the parameter change has resulted in lower levels of effector cells at autoimmunity (e.g., panels (c) and (e)), but has not eliminated the disease completely. Only in cases (d) and (f) has the diseased state been eliminated entirely, consistent with our description above.

3.7.2. Bifurcation diagrams

The effect of an entire range of parameter variation is best summarized with bifurcation diagrams. Using such diagrams, we can consider potential effects of "treatments" that target one or another aspect of the system so as to enable the harmless low avidity T cells, m, to expand and compete with the harmful effector cells, e. For this reason we consider only parameter variations that could ameliorate this protective influence. In Fig. 6(a)–(f), we display the bifurcation diagrams of e with respect to parameters of interest, with all other parameters set at their default values.

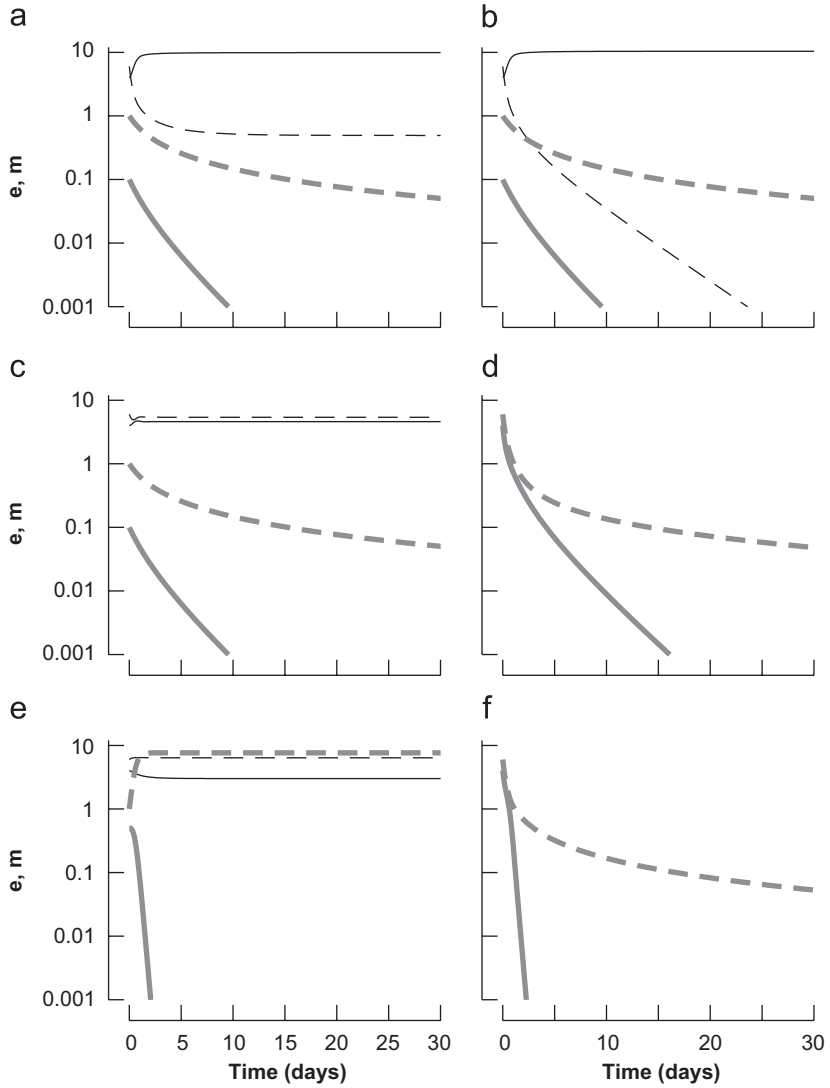

Fig. 5. As in Fig. 4, but showing the evolution over time of $m(t)$ (dashed lines) and $e(t)$ (solid lines) described by system (A.8) and (A.9) from various initial conditions. (Vertical axes are in logarithmic scale; parameter values are identical to those shown in the corresponding panels of Fig. 4). $m(t)$ and $e(t)$ either approach an autoimmune state (black lines) or a healthy state (grey lines). When $\alpha_e = 1$ and $\delta_e = 4\,\text{day}^{-1}$ in panels (d) and (f), respectively, the autoimmune state disappears and $m(t), e(t)$ decay to $\mathbf{S}_1 = (0, 0)$ (the only global attractor).

1(a) Fig. 6(a) summarizes the results of varying the ratio k_m/k_e. Here solid (dashed) lines represent stable (unstable) steady states. For values $0 < k_m/k_e < 2$, only the healthy state $\mathbf{S}_1$ is stable, and there are no T cells in circulation ($m = 0, e = 0$). For significantly larger values of $k_m/k_e \geqslant 11$, two stable steady states coexist, a healthy state $\mathbf{S}_1$ and a diseased state $\mathbf{U}_{1,2}$. The level of m in both states goes to zero (not shown), while nonzero level of effector cells remains in the diseased state.

1(b) Close to $k_m/k_e \approx 2$, a diseased state $\mathbf{S}_2$ appears and becomes stable. For larger k_m/k_e values, e.g., $k_m/k_e \geqslant 3$, the two stable states $\mathbf{S}_1$ and $\mathbf{S}_2$ are separated by a saddle (dashed lines close to zero). Interestingly, the switch in behaviour occurs near a Hopf bifurcation point where an unstable periodic orbit exists at some narrow range of the parameter. This periodic orbit (vertical dotted lines in Fig. 6(a)) acts as a separatrix between the two stable states $\mathbf{S}_1$ and $\mathbf{S}_2$. The behaviour of the effector cells within the range of k_m/k_e corresponding to the above unstable periodic orbit is comparable to the results obtained by Mahaffy and Edelstein-Keshet (2007) and is illustrated in the time plot of Fig. 7.

2. Rates of activation, α_m and α_e, have very different effects on the model. Varying α_m over 40-fold has minimal effect on the diseased state (not shown). In the range $0 \leqslant \alpha_m \leqslant 6$ (day^{-1}), only high level of effector cells occurs ($m = 0$). Beyond that, for $\alpha_m > 6$ (day^{-1}), the growth in memory cell population only lowers, but does not eliminate the level of effector cells. On the contrary, decreasing the effector cell activation rate, i.e., varying α_e over the range $0 \leqslant \alpha_e \leqslant 6$ (day^{-1}), has much more dramatic results, as shown in Fig. 6(b). At $\alpha_e \approx 4\,\text{day}^{-1}$, $\mathbf{S}_2$ and $\mathbf{U}_{1,2}$ exchange stability, and memory cells (not shown) go extinct. Below $\alpha_e \approx 1.5\,\text{day}^{-1}$, a fold bifurcation eliminates the effector cells, leaving only one globally stable healthy state.

3. Fig. 6(c) demonstrates that a similar effect can be obtained by increasing the death rate of effector cells. Here we varied δ_e over the range $0 < \delta_e < 4$ (which includes its default value of $0.3\,\text{day}^{-1}$). As this death rate is increased, exchange of stability between $\mathbf{S}_2$ and $\mathbf{U}_{1,2}$ occurs at $\delta_e \approx 1.8\,\text{day}^{-1}$, while memory cells (not shown) are driven extinct. Beyond this value, effector cells decrease to lower levels, and disappear to a fold bifurcation at $\delta_e \approx 3.7\,\text{day}^{-1}$. At this point, the diseased state $\mathbf{S}_2$ disappears and $\mathbf{S}_1$ becomes a global attractor. By comparison, decreasing δ_m within its normal range of $0 < \delta_m < 0.01$ (day^{-1}), has little effect (not shown), since the default value of this parameter is quite small. Thus the system is more sensitive to changes in the effector cell death rate than to changes in the memory cell death rate.

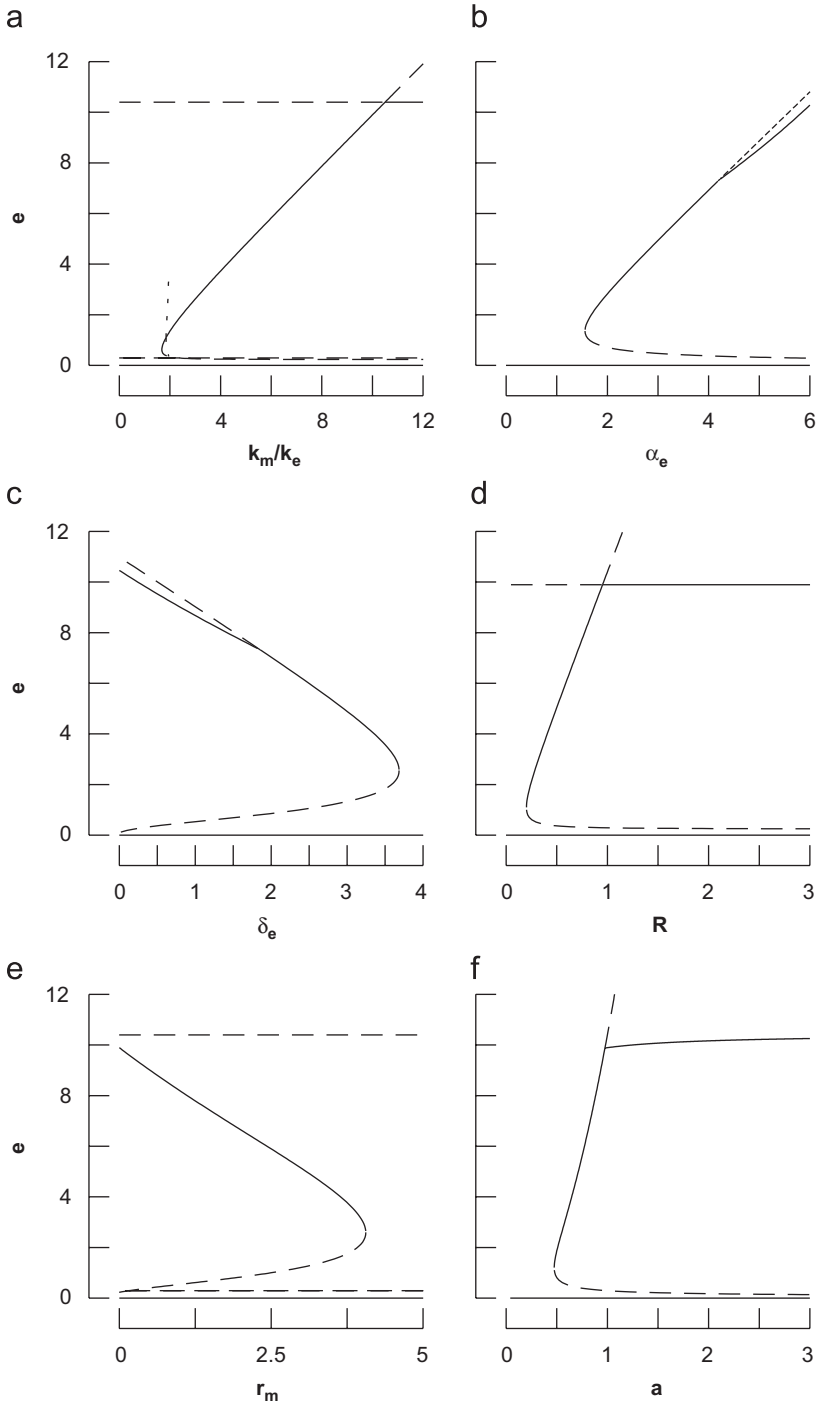

Fig. 6. Bifurcation diagrams of e with respect to (a) the avidity ratio k_m/k_e, (b) the maximum production rate α_e, (c) the turnover rate δ_e, (d) the feedback amplification factor R, (e) the expansion rate r_m, and (f) the fraction of APC population a. Stable steady states are plotted in solid lines while unstable steady states are plotted in dashed lines. Panel (a) shows two branches of unstable periodic orbits (plotted as dotted lines) emerging from a Hopf bifurcation point.

4. The parameter R represents the feedback amplification factor between existing effector cells and activation of new T cells via autoantigen peptide production. Fig. 6(d) shows that decreasing R substantially below 1 peptide-units/cell, leads to the loss of the diseased state to a fold bifurcation. Scaling analysis reveals that increasing R is equivalent to decreasing the competition parameter ε and both k_m and k_e while keeping the ratio k_m/k_e constant.

5. The behaviour of the system under variations of the hypothetical memory cell expansion rate r_m is shown in Fig. 6(e). Increasing r_m over the range $0 \leqslant r_m \leqslant 3$ (day^{-1}) causes incremental expansion in memory cells (not shown) at the expense of effector cells. At $r_m = 4\,\text{day}^{-1}$, a fold bifurcation eliminates the diseased state altogether.

6. It is also possible to target APCs and thereby alter the maximum level of activation α_m and α_e for both populations of T cells. APCs are not an explicit variable yet in the model, but we can approximate the effect of killing APCs by increasing T cell competition (for "sites on APCs") while reducing α_m and α_e. We did this by scaling the maximum activation terms α_m and α_e by a factor a, while scaling the competition term ε^* by the reciprocal $1/a$, where the parameter a is proportional to the level of APCs.

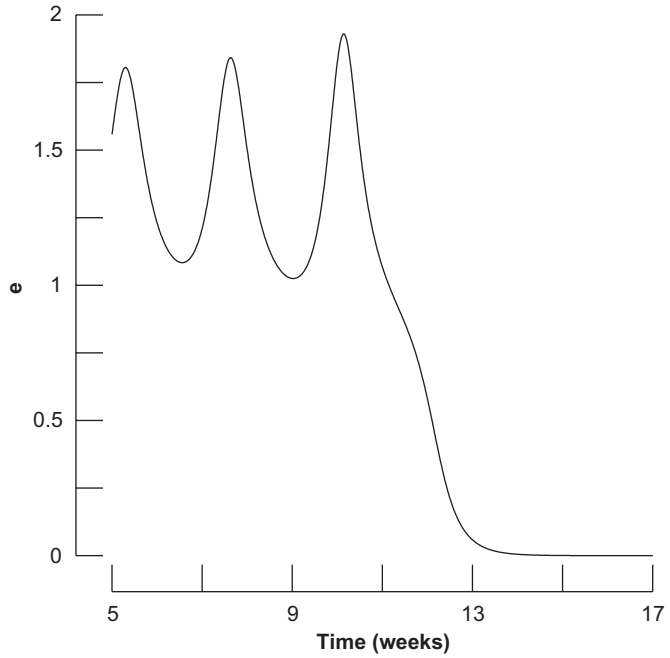

Fig. 7. Cyclic fluctuations in the size of high avidity T cell pool obtained for parameter values given in Table 1 with $k_m/k_e \approx 4$.

Fig. 6(f) shows the bifurcation diagram of e with respect to a. As a decreases, the diseased state is lost to a similar fold bifurcation.

3.7.3. Biological implications

Results of the elementary two-variable model lead to several insights and implications for treatment. We number these points in accordance with the numbering of the results above.

1(a) According to our model, the disparity in avidity has to be large enough for effector cells to take over and cause disease. Otherwise, if $k_e \geqslant k_m/2$, effector cells will not be activated strongly enough to compensate for their higher death rate, and the disease will not take hold. In contrast, if the difference in avidities is very large, e.g., $k_e \ll k_m/10$, then memory cells will be out-competed and eliminated. This finding can be connected to a puzzling experimental observation that treatments aimed at expanding low avidity cells work much better at the acutely diabetic phase.

The T cell clones 17.5, 17.4, and 17.6 studied by Han et al. (2005b) represent a sequence of clones of decreasing avidities. Experimentally, it has been found that the most avid ones (have lowest k_e value), namely 17.5, tend to be weeded out by central tolerance and then undergo further peripheral deletion (Fig. 4 in Han et al., 2005b). This means that the average value of k_e for circulating T cells changes from initially low (highly avid) to slightly higher values, as the 17.4 clone becomes more dominant. This effect leads to a net decrease in k_m/k_e between birth and the stage of acute diabetes as far as the pool of circulating T cells is concerned. (This need not be the case for islet-associated T cells.) According to our result 1(a) above, that decrease could lead to the appearance of memory cells (where previously none could exist). Thus a strategy that involves expanding memory cells would fail initially (because $k_m/k_e > 10$, and there are no memory cells around to expand). However, at later stages (once $k_m/k_e \leqslant 10$), a few memory cells are present, and thus memory cell expansion could be an effective treatment strategy. This explains why treatments aimed at expanding low avidity T cells are seen to be very effective at the acute phase of the disease, and not at all in the earlier, prediabetic stage.

1(b) Finding a Hopf bifurcation and a periodic orbit that induces a series of fluctuations in the T cell levels (Fig. 7), is reminiscent of the dynamics quantified by Trudeau et al. (2003) and modeled by Mahaffy and Edelstein-Keshet (2007). These oscillations have increasing period and amplitude, and eventually settle down to the disease-free state. Even though the populations of T cells eventually decay to near-zero level, the transiently elevated level of e could severely kill or damage β cells, possibly leading to full blown diabetes. Recall the implications to relapse-remission of the disease proposed by von Herrath et al. (2007).

2. We found that lowering the APC-mediated rate of expansion of effector cells, α_e, is much more effective at eliminating the disease than increasing the APC-mediated expansion of low avidity memory cells α_m to bias competition. Changing memory cell expansion by a factor of over 40, only reduces circulating effector cell levels by a factor of 5 and does not eliminate the disease. This suggests that killing APCs (which reduces both α_e and α_m) is a better treatment strategy than solely increasing α_m.

3. Our investigation of treatments that target the mortality rates (δ_m and δ_e) of T cells reveals that strategies that increase effector cell mortality are much more effective than those that reduce memory cell mortality. It remains to be seen whether such treatments can be devised.

4. The parameter R represents an aggregate of many processes, from the apoptosis of β cells to the processing and presentation of their components as p-MHC on APCs. Reduction of R could presumably be accomplished by protecting pancreatic islets, e.g., by crowding out effector cells. This motivates a later discussion of such a role for low avidity T cells. R could also be reduced by treatments that lead to more rapid and effective clearance of apoptotic β cells, as this would effectively shut down the positive feedback cycle that is set up via autoantigen in autoimmunity. Previous work has indicated that macrophage clearance of apoptotic cells is defective (e.g., in NOD mice). Thus treatments that address such defects can be beneficial by indirectly reducing R.

5. We found that a plausible treatment strategy of expanding memory cell pool by artificial means can lead to better prognosis, by competitively reducing effector cell levels and eventually eliminating the disease. In the context of the simple model, the expansion rate, r_m, has to be significant (on average, a single memory cell producing four or more progeny per day) for a complete cure. An important point is that this expansion can only be affected at a stage of the disease when memory cells are present. This suggests either waiting for the average avidity to decline (see point 1(a)), or better still, manipulating other parameters to shift the system into a regime where memory cells are present.

6. Treatments that target APCs affect multiple aspects of the model. Overall, a large enough depletion of APCs can eliminate autoimmunity by reducing the proliferation rates and increasing competition between T cells. Our model suggests that this is a viable strategy for a "cure", provided that a sufficiently large APC depletion can be executed.

4. Including APCs in the model

We extend the two-variable model of system (12) and (13) by including APCs as a dynamic variable. This allows us to test hypothesis II which suggests that low avidity T cells delete APCs (we also examine Result 6 in an expanded setting). Accordingly, we consider an equation for A, the level of APCs, as follows:

$$\frac{dA}{dt} = \sigma_a - k_a MA - \delta_a A \tag{16}$$

where σ_a is the basal rate of production of APCs from precursors, assumed constant, δ_a is the turnover rate of APCs, and $k_a \geqslant 0$ is the killing rate of APCs per low avidity T cell, if any. Estimates for the parameters in this model are derived in Appendix B. To account for the effects of APCs on T cells, we have modified Eqs. (12) and (13) in the following two ways: (1) We first considered the case that $\alpha_i = \overline{\alpha}_i A$, for $i = m, e$, i.e., the activation of T cells is directly proportional to the level of APCs. (2) We also considered the above together with $\varepsilon = \overline{\varepsilon}/A$ (and similar variants) to indicate that the competition is affected by the availability of sites on APCs.

In the absence of memory cells, APCs settle at the steady state level $A_d = \sigma_a/\delta_a > 0$. We used this value to rescale the variable so that $a = A/A_d$, where $0 < a \leqslant 1$, as shown in Appendix A (Eqs. (A.10)–(A.12)). We first examined the dynamics of this model for $r_m = 0$, and asked how the killing rate, k_a, affects its behaviour. Surprisingly, varying k_a over several 10-fold factors has negligible effect on the level of e in the diseased state, e_d, but dramatic effects on the level of m_d (diagrams not shown). Indeed, plots of e_d vs k_a are nearly indistinguishable from $e_d \sim C$ for some constant C, whereas m_d shows an inversely proportional behaviour to k_a, i.e., $m_d \sim 1/k_a$. The trend is observed for both cases (1) and (2) above. This trend can be explained by noting that at steady state, in terms of the scaled variables, Eq. (16) implies $a_d = 1/(1 + k_a m_d)$, while the modified Eqs. (12) and (13) lead to the revised steady-state model $a_d(\alpha_e^* f_e(e_d) - \alpha_m^* f_m(e_d)) = \delta_e - \delta_m$. In the parameter regime of the model, the latter constraint is closely approximated by the curve $a_d \approx \delta_e/(\alpha_e^* e_d^2)$. This means that large changes in a_d hardly affects the value of e_d, but do affect the value of m_d much more strongly. This result suggests that the efficacy of killing of APCs by low avidity T cells ordinarily has little protective role, as increasing its per-cell APC-killing rate quickly damps out the level of the low avidity population with minimal change in the effector population level.

We then asked how a treatment that amplifies low avidity T cell population via r_m, i.e., artificially enhancing proliferation (with no APC involvement), would affect the behaviour. Fig. 8 displays the bifurcation diagram of e (according to system (A.10)–(A.12)) with respect to the expansion parameter r_m when both activation and competition are affected by a (Case 2). Case 1 is qualitatively quite similar. The resemblance to Fig. 6(e) is apparent. Healthy and autoimmune states coexist up to some memory cell expansion rate. Beyond that value, the diseased state disappears. In this treatment scenario, expanding low avidity T cells successfully reduces the level of APCs and effector cells significantly. The APC-independent expansion of low avidity T cells is essential for this to work. Overall, we conclude from this analysis that including APCs as a dynamic variable does not significantly change the previous qualitative predictions of the reduced model. If low avidity T cells kill APCs, treatments that make this killing more efficacious are seen to be futile, but expanding those low avidity cells artificially can be beneficial.

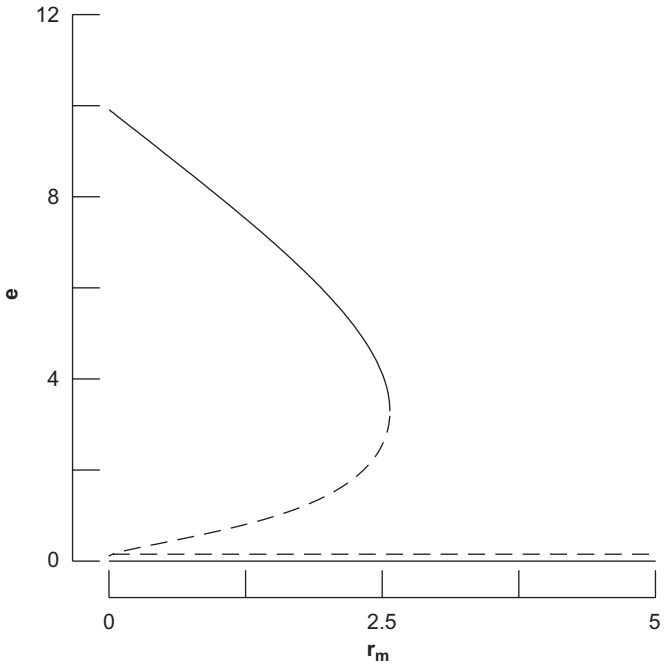

Fig. 8. Bifurcation diagram of e with respect to r_m according to system (A.10)–(A.12). Observe that the healthy state becomes a global attractor due to the deletion of a sizable portion of APCs by an expanded population of low avidity T cells. At the threshold value $r_m \approx 2.57\,\text{day}^{-1}$, the autoimmune state disappears.

5. β cell model

The detailed dynamics of β cells is not well characterized. It has been demonstrated recently that new β cells appear in NOD mice after birth, but their source remains controversial. While some experimental evidence suggests β cell neogenesis from precursor cells (such as stem cells and ductal cells) (Bonner-Weir, 2001; Finegood et al., 1995; Thyssen et al., 2006), others suggest β cell replication from already existing proliferative β cells (Bock et al., 2003; Dor et al., 2004; Finegood et al., 1995; Jo et al., 2007; Sreenan et al., 1999; Teta et al., 2005). We considered several variants of an equation for the population of β cells in order to further test both hypotheses pertaining to the role of low avidity T cells, notably their putative protective effect in islets. Of all variants tested, the one found most satisfactory closely follows a model developed by the group of Vered Rom-Kedar (with Roi Malka, PhD student, Weizmann Institute) in an unrelated biological setting. We revised it to arrive at the equation for β cells,

$$\frac{dB}{dt} = s\frac{B}{k_B + B} - dB + \frac{\kappa EB}{1 + \mu_0 B + \mu_1 M} \tag{17}$$

where s is the maximal number of new β cells generated per day, k_B is the β cell level for half-maximal renewal rate, d is the turnover rate of β cells per day, κ is the killing rate of β cells by effector cells per day, μ_0 is a per-β cell saturation parameter for β cell killing, while $\mu_1 M$ is the inhibition term exerted by the very small fraction of low avidity T cells on the killing of β cells in the islets. The first two terms in Eq. (17) represent normal β cell dynamics, and possess two steady state ($B = 0$ and $B_h = (s - k_B d)/d$). We note that as the number of β cells decreases (e.g., due to killing in an autoimmune attack or after an apoptotic wave), the growth rate per β cell (term 1) increases (Sherry et al., 2006; Finegood et al., 1995; Teta et al., 2005). In this sense, the first term could represent enhanced growth rate at low population due to stress-dependent effects.

The two states of interest, according to this model, are the healthy state $(0, 0, B_h)$, where B_h is the number of β cells in nondiabetic NOD mice, and the diseased state (M_d, E_d, B_d), where $E_d \gg M_d \geqslant 0$ and $B_d > 0$. By rescaling the variable B by B_h so that $b = B/B_h$ (and rescaling M and E by K_e, see Eqs. (A.13)–(A.16) in Appendix A), the level of β cells becomes $b_h = 1$ in the healthy state and $b_d = B_d/B_h$ in the diseased state. As shown schematically in Fig. 9, b_d lies at the intersection of the curves $q_1(b) \equiv \kappa^* eb/(1 + \mu_0^* b + \mu_1^* m)$ and $q_2(b) \equiv s^* b/(k_b + b) - \mathrm{d}b$. Since ~90% of β cells are killed during the autoimmune attack, it is expected that $b_d \approx 0.1 b_h$. In Appendix B, we use this latter result together with some additional experimental results obtained in Teta et al. (2005), Magami et al. (2002), Bock et al. (2003), Marée et al.

(2006a), Jo et al. (2007), Dor et al. (2004) and Finegood et al. (1995) to estimate the remaining parameters appearing in Eqs. (A.15) and (A.16).

5.1. Biological implications and treatments

Our two main objectives in this section are: (1) to determine the effects of low and high avidity T cells on the general dynamics of β cells; and (2) to examine those treatments that are linked to hypotheses (I) and (II) described above. In order to do so, we use the parameter values listed in Table 1 and system (A.13)–(A.16). The main obstacle facing us here is that we do not have any prior knowledge of the values of the parameters $s^* = s/B_h$, $k_b = k_B/B_h$ and $R^* = \bar{R}B_h$ appearing in this system. Bifurcation diagrams can be used, however, to determine the parameter-regimes in which the model is most consistent with experimental results. Fig. 10(a) shows the bifurcation diagram of b with respect to the ratio s^*/k_b. It demonstrates that in order to attain an autoimmune state in the range of $b_d \approx 0.1$ (with $m \approx m_d = 0.5$ and $e \approx e_d = 10$), the ratio s^*/k_b should be in the range of $[0.07, 0.08]$ (day^{-1}). (An expanded range would correspond to a less acute loss of β cells which is seen in some cases of T1D.) Similarly, we may estimate the parameter regime for R^* and obtain the range $[159, 186]$ in peptide-units/cell.

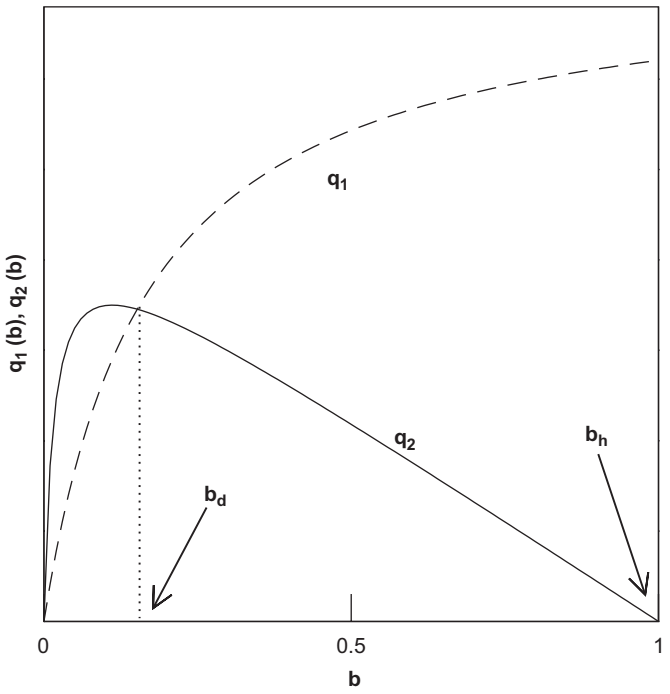

Fig. 9. Graphs of the functions q_1 (dashed line) and q_2 (solid line). They represent, according to Eq. (17), the killing and natural dynamics of β cells, respectively. The points $b_h = 1$ and $b_d \approx 0.1$ represent the level of β cells in the healthy and autoimmune diseased states, respectively.

Using these fitted values, we are ready to determine how the model behaves in view of hypotheses (I) and (II). Since hypothesis (I) suggests that the expanded population of low avidity T cells crowd the islets and inhibit the killing of β cells, we investigate the influence of the expansion parameter r_m on the general dynamics of β cells.

Fig. 10(b) shows similar features to those observed previously in the two-variable and the APC models discussed earlier; the bifurcation diagram reveals that the level of β cells in the diseased state increases rapidly as r_m increases until the diseased state disappears, leaving the healthy state as the only stable steady state. The loss of the diseased state is reminiscent of the disappearance of high avidity T cells, demonstrated in Figs. 6(e) and 8. The rapid increase, however, seemed to be not very consistent with the experimental observation.

The model shows sensitive dependence on r_m which makes hypothesis (I) less likely to occur. Hypothesis (II), on the other hand, produces results more consistent with the experiment. In view of case 2 discussed in Section 3, hypothesis (II) can be modeled by scaling ε^* by a factor of $1/a$ while scaling α_m and α_e by a factor of a, where a is the fraction of APCs circulating in the lymph nodes. The resulting bifurcation diagram of b with respect to a, shown in Fig. 10(c), is very similar to what we have seen previously. The coexistence of the healthy state $(0, 0, 1)$ and diseased state (m_d, e_d, b_d) persists until the level of APCs, a, becomes sufficiently small. The figure also shows two connected branches of stable steady states corresponding to the diseased states $\mathbf{S}_1$ (semi-horizontal branch) and $\mathbf{U}_{1,2}$ (semi-vertical branch) obtained from the two-variable model. We may conclude that within a 2-fold decrease in the value of a, a slow increase in the level of β cells in the diseased state, b_d, is observed. One could also observe a significant increase in b_d when a decreases by over 2-fold as the diseased state first enters the semi-vertical branch and then disappears to a fold bifurcation at $a \approx 0.25$. This feature suggests that hypothesis (II) is the likely candidate for the type of effect low avidity T cells may exert in T1D.

The bifurcation diagram corresponding to the parameter μ_1 displays results similar to those obtained for the parameter k_a in the previous section (results not shown). The plot of b_d with respect to this parameter shows that $b_d \sim C_1$, for some constant C_1,

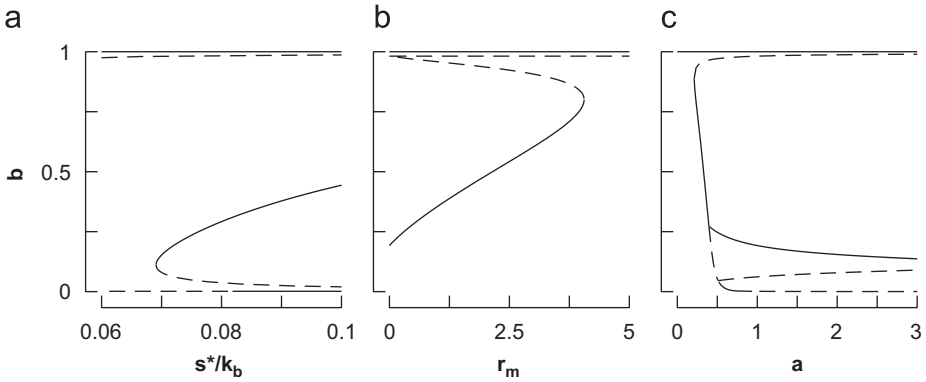

Fig. 10. Bifurcation diagrams of B with respect to the parameters (a) s^*/k_b; (d) r_m; and (c) a. Stable (solid lines) and unstable (dashed lines) steady states are shown. Panel (a) shows a physiologically reasonable parameter range for r, while (b) and (c) elucidate the effects of hypotheses (I) and (II).

while the plots of e_d and m_d show that $e_d \sim \mu_1/(C_2+\mu_1)$ and $m_d \sim 1/\mu_1$ for some constant C_2.

6. Discussion

We have explored in this paper the role of high and low avidity populations of IGRP-reactive T cells in the progression and treatment of Type 1 Diabetes (T1D). To do so, we introduced a two-variable model describing the dynamics of these two competing populations of T cells. The model is compatible with the idea that the low avidity T cells are immunoregulatory. We showed that two coexisting stable steady states are attained: a healthy state (from which we subtracted any normal basal background level of autoreactive T cells), and an autoimmune state in which the size of the high avidity T cell population is large.

Other well-known autoantigens in T1D include insulin, proinsulin, GAD, HSP65 and others. The paradigm described by this model has been confirmed to work also for a much smaller $CD8^+$ T cell subpopulation targeting a subdominant epitope on dystrophia myotonica kinase, a diabetes-relevant autoantigen that is expressed systemically (Tsai et al., 2008). Given the observations on these two very different autoreactive T cell subsets, it is reasonable to expect that our model would extend to most other autoantigenic specificities in diabetes and, possibly, to other autoimmune diseases. As described below, we are extending the analysis to consider the possible roles of competing subdominant T cell clones in a follow-up manuscript.

We have examined two hypotheses proposed for how low avidity T cells play a protective role in T1D (Tsai et al., 2008). In principle, there are other possibilities for the underlying mechanism that were not discussed in this paper. These include the release of immunosuppressive mediators, niche competition for IL-2, bystander suppression, expansion of natural regulator T cells, and/or promotion of a regulatory phenotype of APCs. We can reject many of these based on experimental evidence from the Santamaria Laboratory. First, immunoregulation by the low avidity clones is cell contact-dependent (at least *in vitro*), excluding immunoregulatory cytokines or competition for IL-2 (between regulators and effectors) as mediators of suppression. Second, the immunoregulatory low avidity clones do not produce or secrete immunoregulatory cytokines (e.g., TGFb, IL-4, IL-10). We also have evidence that the expansion of low avidity memory-like cell pool is not accompanied by the expansion, or recruitment to the site of immunoregulation, of natural Tregs (i.e., $CD4^+$ $CD25^+FoxP3^+$ cells). Furthermore, we have documented that these memory low avidity clones can readily kill APCs, both *in vitro* and *in vivo*, i.e., that they play an immunoregulatory role.

We cannot exclude the possibility that the interaction between these T cells and the APCs may also promote a regulatory phenotype of APCs. However, if this effectively leads to a reduction in the activation parameters α_i, it will qualitatively produce similar outcomes to our models. Based on such evidence, we have considered here only two main hypotheses; namely, low avidity T cells either (I) crowd the islets in the pancreas, or (II) kill APCs responsible for activating T cells. To test these hypotheses, we initially used the two-variable model, then extended it to three variables, first by including APCs, and then by including β cells. In reality, the two versions of the three-variable models are not mutually exclusive and further exploration of more complete versions are forthcoming.

Our results reveal that hypothesis (II) is more plausible. In particular, we found a discrepancy between the observed experimental results and the outcome of hypothesis (I) applied to the three-variable β cell model. Testing whether low avidity T cells crowd the islets, we have observed that the level of β cells in the diseased state, b_d, rapidly increases with increasing expansion rate of low avidity T cells, r_m (i.e., b_d was quite sensitive to variations in r_m, a feature not observed experimentally). This suggests that the killing of APCs by low avidity T cells is the dominant effect, since b_d is less sensitive to variations in the number of APCs. Only when the number of APCs is reduced by over 2-fold in the model, does the healthy state become globally stable, a result more consistent with experiments.

It has been suggested by Han et al. (2005b) that autoimmune inflammation preferentially fuels the local expansion of the highest avidity and the most pathogenic T cell pool, but systemic tolerance selectively decreases the size of this pool causing prevalent recruitment of low avidity clonotypes at the primary autoimmune response. In other words, the avidity ratio k_m/k_e between the two populations of circulating T cells is not a constant quantity but rather a dynamic one that decreases with the depletion of the high-avidity (17.5) pool. We have established that, before selective tolerance, the avidity ratio between the two populations is large and the size of low avidity T cell population in the autoimmune state is either zero or very small. Therefore, any treatment aimed at expanding the size of this population *at this stage* will not be effective as has been demonstrated experimentally (Tsai et al., 2008). On the other hand, the model shows that the depletion of the highly avid pool of cells (which is equivalent to increasing k_e) elevates the level of low avidity T cells, enabling certain treatments at the later stage of the disease to expand this population. This explains why treatments applied at this later stage will be more effective.

Strategies for treating autoimmune diseases include manipulation (and expansion of) regulatory T cells. Our model is compatible with this goal, and indeed, the new avenue described by Tsai et al. (2008) points to the promise of a philosophically similar strategy, showing that this can restore normoglycemia in newly diabetic mice. However, while the memory-phenotype autoreactive T cells that arise from low avidity naive precursors are immunoregulatory, they differ from conventional Tregs ($FoxP3^+CD4^+CD25^+$ T cells), but share some similarities with them. For example, they cannot make IL-2 and do not proliferate in response to antigenic stimulation *in vitro* in the absence of exogenous cytokines.

Thehealthy and autoimmune states discussed in this paper represent the long term behaviour of the models considered. The models provide insights as to what types of treatment strategies could work. However, we are still far from a well-characterized and sufficiently complete model to adequately test treatment regimes (doses, frequency and types of interventions). For this, we are currently considering more detailed and more complete simulation models that build on those described here. For example, it has been observed experimentally (unpublished work) that treatments targeting IGRP-reactive T cells could either downgrade or expand T cells with other specificities. The outcome depends on the type, timing, and details of the treatment. An extended model consisting of both IGRP-reactive T cells and CTLs with other specificities is currently under development. That expanded model is being used to generate more realistic scenarios, and to investigate specific treatment regimes with the eventual goal of optimizing the type, dose and the frequency of treatment protocols.

It is important to note that the transient behaviour (and not just the existence of the diseased states) is quite influential. For example, as in Trudeau et al. (2003) and in the previous model by Mahaffy and Edelstein-Keshet (2007), we showed that large cyclic fluctuations in effector cells can occur in certain cases (see Fig. 7). Even though the system eventually reaches the healthy state, the fluctuations may cause enough damage to the number of β cells to cause acute T1D. When designing a treatment strategy, it is

important to do so carefully to avoid such cyclic fluctuation regimes. As mentioned earlier, we can also connect such cyclic dynamics to the phenomena of remission and relapse that have been described by von Herrath et al. (2007). The autoimmune disease process activates high-avidity clones, which turn into β cell killers and then die, but also turns low avidity clones into APC-killer memory-phenotype cells which then attempt to shut down the process. Once the suppressors go away, a new wave of disease-promoting and disease-suppressing events can arise. The fact that the disease generates a negative feedback regulatory loop that attempts to counter disease progression could be considered a relapsing-remitting event. (That said, as in many other nonlinear phenomena, cyclic dynamics occur only in specific ranges of parameter settings, and was not our primary focus here.)

Acknowledgements

The authors gratefully acknowledge funding by the Mathematics of Information Technology and Complex Systems (MITACS) Canada, and by the Juvenile Diabetes Research Foundation (JDRF). P. Santamaria contribution is funded by the Canadian Institutes of Health Research, the Canadian Diabetes Association and the JDRF. P. Santamaria is a Scientist of the Alberta Heritage Foundation of Medical research (AHFMR) and a JDRF Scholar. Discussion with Professor V. Rom-Kedar (Weizmann Institute of Science) greatly benefited our development of Section 5. We thank an anonymous reviewer for comments that helped to improve the paper.

Appendix A. Theoretical results

A.1. Stability analysis, two-variable model

The Jacobian matrix of system (6) and (7) is

$$J=\begin{pmatrix} F+MF_M & MF_E \\ EG_M & G+EG_E \end{pmatrix}$$

At the equilibrium point $\mathbf{S}_1$ and $\mathbf{S}_2$, these are

$$J_{\mathbf{S}_1}=\begin{pmatrix} F(\mathbf{S}_1) & 0 \\ 0 & G(\mathbf{S}_1) \end{pmatrix} \quad \text{and} \quad J_{\mathbf{S}_2}=\begin{pmatrix} M_2F_M(\mathbf{S}_2) & M_2F_E(\mathbf{S}_2) \\ E_2G_M(\mathbf{S}_2) & E_2G_E(\mathbf{S}_2) \end{pmatrix}$$

At $\mathbf{S}_1$, the eigenvalues are $\lambda_1=F(\mathbf{S}_1)$ and $\lambda_2=G(\mathbf{S}_1)$, so $\mathbf{S}_1$ is a stable node whenever $F(\mathbf{S}_1), G(\mathbf{S}_1)<0$ and unstable otherwise. For stability of $\mathbf{S}_2$, we require

$$\mathrm{tr}(J_{\mathbf{S}_2})=M_2F_M(\mathbf{S}_2)+E_2G_E(\mathbf{S}_2)<0 \tag{A.1}$$

$$\det(J_{\mathbf{S}_2})=M_2E_2[F_M(\mathbf{S}_2)G_E(\mathbf{S}_2)-F_E(\mathbf{S}_2)G_M(\mathbf{S}_2)]>0 \tag{A.2}$$

But $M_2, E_2>0$, so inequality (A.2) reduces to

$$F_M(\mathbf{S}_2)G_E(\mathbf{S}_2)-F_E(\mathbf{S}_2)G_M(\mathbf{S}_2)>0 \tag{A.3}$$

By inequalities (8) and (A.3), we have

$$F_M(\mathbf{S}_2)G_E(\mathbf{S}_2)+|G_M(\mathbf{S}_2)|F_E(\mathbf{S}_2)>0$$
$$\Longrightarrow |G_M(\mathbf{S}_2)|F_E(\mathbf{S}_2)>-F_M(\mathbf{S}_2)G_E(\mathbf{S}_2)=|F_M(\mathbf{S}_2)|G_E(\mathbf{S}_2)$$

In other words,

$$\frac{F_E(\mathbf{S}_2)}{|F_M(\mathbf{S}_2)|}>\frac{G_E(\mathbf{S}_2)}{G_M(\mathbf{S}_2)} \tag{A.4}$$

Similarly, by inequality (A.1), we have

$$E_2G_E(\mathbf{S}_2)<-M_2F_M(\mathbf{S}_2)=M_2|F_M(\mathbf{S}_2)|\Longrightarrow G_E(\mathbf{S}_2)<\frac{M_2}{E_2}|F_M(\mathbf{S}_2)|$$

If D_m and D_e are the slopes of the tangent lines to the nullclines $F(M,E)=0$ and $G(M,E)=0$, respectively, then these slopes satisfy

$$D_m=\frac{\mathrm{d}M}{\mathrm{d}E}=-\frac{F_E}{F_M}=\frac{F_E}{|F_M|}, \quad D_e=\frac{\mathrm{d}M}{\mathrm{d}E}=-\frac{G_E}{G_M}=\frac{G_E}{|G_M|} \tag{A.5}$$

It follows from (A.4) and (A.5) that the steady state $\mathbf{S}_2$ is stable if and only if the inequalities in (9) are satisfied.

At $\mathbf{U}_1$ and $\mathbf{U}_2$, the Jacobian is

$$J_{\mathbf{U}_1}=\begin{pmatrix} F(\mathbf{U}_1) & 0 \\ \mathscr{E}_1G_M(\mathbf{U}_1) & \mathscr{E}_1G_E(\mathbf{U}_1) \end{pmatrix} \quad \text{and}$$

$$J_{\mathbf{U}_2}=\begin{pmatrix} \mathscr{M}_2F_M(\mathbf{U}_2) & \mathscr{M}_2F_E(\mathbf{U}_2) \\ 0 & G(\mathbf{U}_2) \end{pmatrix}$$

The eigenvalues for $\mathbf{U}_1$ are $\lambda_1=F(\mathbf{U}_1)$ and $\lambda_2=\mathscr{E}_1G_E(\mathbf{U}_1)$. This implies that $\mathbf{U}_1$ is stable whenever $F(\mathbf{U}_1)<0$ and $G_E(\mathbf{U}_1)<0$. At $\mathbf{U}_2$, the eigenvalues are $\lambda_1=\mathscr{M}_2F_M(\mathbf{U}_2)$, which is negative in view of inequalities (8), and $\lambda_2=G(\mathbf{U}_2)$. Thus $\mathbf{U}_2$ is stable whenever $G(\mathbf{U}_2)<0$.

When $\mathrm{tr}(J_{\mathbf{S}_2})=0$ and $\det(J_{\mathbf{S}_2})>0$, the eigenvalues become pure imaginary and the equilibrium point $\mathbf{S}_2$ turns into a Hopf bifurcation point. This is equivalent to (10).

A.2. Explicit two-variable model

Existence of the diseased state ($\mathbf{S}_2$): Fig. 2(b) reveals that inequality (15) is satisfied whenever $E<\bar{E}$. Let $g(E)\equiv \alpha_m f_m(E)-\alpha_e f_e(E)$. Then $g(0)=g(\bar{E})=0$ and $g(E)<0$, for $0<E<\bar{E}$. By the Mean Value Theorem, the function $g(E)$ must possess a local minimum at $E=\tilde{E}$. Since

$$g'(E)=\frac{n\alpha_m k_m E^{n-1}}{(k_m^n+E^n)^2}-\frac{n\alpha_e k_e E^{n-1}}{(k_e^n+E^n)^2}$$

it follows that

$$\frac{\alpha_m k_m}{(k_m^n+\tilde{E}^n)^2}-\frac{\alpha_e k_e}{(k_e^n+\tilde{E}^n)^2}=0 \iff \left[\frac{(k_e^n+\tilde{E}^n)}{(k_m^n+\tilde{E}^n)}\right]^2=\frac{\alpha_e k_e}{\alpha_m k_m} \tag{A.6}$$

But the quadratic expression in (A.6) is a strictly increasing function of $\tilde{E}$ and

$$\frac{k_e^n}{k_m^n}\leqslant\left[\frac{(k_e^n+\tilde{E}^n)}{(k_m^n+\tilde{E}^n)}\right]^2<1$$

Thus

$$\frac{k_e^n}{k_m^n}<\frac{\alpha_e k_e}{\alpha_m k_m}<1 \iff \left(\frac{k_m}{k_e}\right)^{n-1}>\frac{\alpha_m}{\alpha_e}>1 \tag{A.7}$$

must hold. Inequality (A.7) is useful in specifying a lower bound on the ratio (k_m/k_e) which is not known experimentally. Since there is only one positive solution to Eq. (A.6), the point $E=\tilde{E}$ is the only local minimum in the interval $[0,\bar{E}]$. If $g(\tilde{E})>\delta_m-\delta_e$, then no equilibrium points exist; at $g(\tilde{E})=\delta_m-\delta_e$, there is a bifurcation point beyond which two equilibrium points exist.

Scaling the two-variable model: We scale M and E in system (12) and (13) by applying the substitution $m=M/k_e$ and $e=E/k_e$. The resulting equations are given by

$$\frac{\mathrm{d}m}{\mathrm{d}t}=m\left[\alpha_m\frac{e^n}{(k_m/k_e)^n+e^n}-\delta_m-\varepsilon^*(m+e)\right] \tag{A.8}$$

$$\frac{\mathrm{d}e}{\mathrm{d}t}=e\left[\alpha_e\frac{e^n}{1+e^n}-\delta_e-\varepsilon^*(m+e)\right] \tag{A.9}$$

where $\varepsilon^*=\varepsilon k_e$. Notice that the relative avidities of the T cells in both populations is expressed in this model by the ratio k_m/k_e appearing in Eq. (A.8). System (A.8) and (A.9) has been used in plotting all the figures of Section 3.7.

Scaling the APC model: By setting $m = M/k_e$, $e = E/k_e$ and $a = A/A_d = A\delta_a/\sigma_a$, we obtain

$$\frac{dm}{dt} = m\left[\alpha_m^* a \frac{e^n}{(k_m/k_e)^n + e^n} + r_m - \delta_m - \frac{\bar{\varepsilon}^*}{a}(m+e)\right] \tag{A.10}$$

$$\frac{de}{dt} = e\left[\alpha_e^* a \frac{e^n}{1+e^n} - \delta_e - \frac{\bar{\varepsilon}^*}{a}(m+e)\right] \tag{A.11}$$

$$\frac{da}{dt} = \delta_a(1 - k_a^* m a - a) \tag{A.12}$$

where $\alpha_i^* = \bar{\alpha}_i\sigma_a/\delta_a$, for $i = m, e$, $\bar{\varepsilon}^* = \bar{\varepsilon}k_e\delta_a/\sigma_a$, and $k_a^* = k_a k_e/\delta_a$.

Scaling the β cell model: By setting $m = M/K_e$, $e = E/K_e$, $b = B/B_h$ and $p = P/K_e$, where $B_h = (s - dk_B)/d$ is the healthy state of B, we obtain

$$\frac{dm}{dt} = m\left[\alpha_m \frac{p^n}{(K_m/K_e)^n + p^n} + r_m - \delta_m - \varepsilon^*(m+e)\right] \tag{A.13}$$

$$\frac{de}{dt} = e\left[\alpha_e \frac{p^n}{1+p^n} - \delta_e - \varepsilon^*(m+e)\right] \tag{A.14}$$

$$\frac{db}{dt} = s^* \frac{b}{k_b + b} - \left(d + \frac{\kappa^* e}{1 + \mu_0^* b + \mu_1^* m}\right) b \tag{A.15}$$

$$p = \frac{R^* be}{1 + \mu_0^* b + \mu_1^* m} \tag{A.16}$$

where $s^* = s/B_h$, $k_b = k_B/B_h$, $\kappa^* = \kappa K_e$, $\varepsilon^* = \varepsilon K_e$, $\mu_0^* = \mu_0 B_h$, $\mu_1^* = \mu_1 K_e$ and $R^* = \bar{R}B_h$. In this case, the healthy steady state of b is $b_h = 1$ and the ratio $K_m/K_e = k_m/k_e$.

Appendix B. Parameter Estimation

Here we show details of estimates for parameters appearing in system (12) and (13). We used previous parameter estimates in Mahaffy and Edelstein-Keshet (2007) to deduce that $\alpha_m \approx 11\text{day}^{-1}$. This value agrees with the experimental estimate of 10–20 day^{-1} (Veiga-Fernandes et al., 2000).

The turnover rates of M and E are $\delta_m = 0.01$ and $\delta_e = 0.3$ day^{-1} (Marée et al., 2006b). Finally, the total number of low and high avidity T cells at the autoimmune state is estimated experimentally to be $M_d \approx 10^4 - 10^5$ and $E_d \approx 10^6$ cells (Mahaffy and Edelstein-Keshet, 2007). These data together with inequalities (14) can help us evaluate the remaining parameters in system (12) and (13). Assume that $E_d \gg k_e$, which is the case for diabetic NOD mice. It follows that at steady state

$$\alpha_m \frac{E_d^n}{k_m^n + E_d^n} - \delta_m - \varepsilon(M_d + E_d) = 0 \tag{B.1}$$

$$\alpha_e - \delta_e - \varepsilon(M_d + E_d) = 0 \tag{B.2}$$

Using Eqs. (B.1) and (B.2), we may conclude that

$$\alpha_m \frac{E_d^n}{k_m^n + E_d^n} = \delta_m + \alpha_e - \delta_e \tag{B.3}$$

There are three cases to consider.

1. $E_d \gg k_m$. In this case Eq. (B.1) becomes

$$\alpha_m - \delta_m = \varepsilon(M_d + E_d) \iff E_d \approx \frac{\alpha_m - \delta_m}{\varepsilon}$$

But from inequalities (14) and (B.3), we have $0 < \alpha_m - \alpha_e = \delta_m - \delta_e < 0$, which is a contradiction. Therefore this case is rejected.

2. $E_d \approx k_m$. This implies that $\frac{\alpha_m}{2} - \delta_m \approx \varepsilon(M_d + E_d) \Longleftrightarrow M_d + E_d \approx \frac{\alpha_m/2 - \delta_m}{\varepsilon}$, hence, by Eq. (B.2),

$$\frac{\alpha_m}{2} \approx \delta_m - \delta_e + \alpha_e \tag{B.4}$$

3. $E_d \ll k_m$. It follows from Eq. (B.3) that

$$\frac{\alpha_m E_d^n}{k_m^n} = \delta_m - \delta_e + \alpha_e \iff \frac{\alpha_m E_d^n}{k_m^n} - \delta_m = \varepsilon(M_d + E_d) \tag{B.5}$$

In view of Eqs. (B.2) and (B.4) and the parameter values stated above (including M_d and E_d), case 2 reveals that

$$\left\{\begin{array}{l} \frac{\alpha_m}{2} - \alpha_e = \delta_m - \delta_e \\ M_d + E_d = \frac{\alpha_e - \delta_e}{\varepsilon} \end{array}\right\} \Longrightarrow \left\{\begin{array}{l} \frac{[10-20]}{2} - \alpha_e = -0.29 \\ \frac{\alpha_e - 0.3}{\varepsilon} = 0.5 \times 10^5 + 10^6 \end{array}\right\}$$

where square brackets hereafter will symbolize parameter ranges. It follows that $\alpha_e \approx [5-10]\,\text{cell}^{-1}$ and $\varepsilon \approx [5-10] \times 10^{-6}$ $(\text{cell day})^{-1}$. By using these values and setting $n = 2$, we deduce from Eq. (B.5) in case 3 that $k_m \approx 1.4 \times 10^6$ in T cell units (the two extreme values of α_m and α_e generate the same value for k_m).

The parameters k_m and k_e are aggregate quantities representing many complex interactions at the molecular level between TCRs and p-MHC. It is not easy to measure these values directly. However, we can use information about functional avidity to estimate their ratio. According to Han et al. (2005b), the $\text{IGRP}_{206-214}$ concentration that gives the half-maximum response for IL-2 (cytokine) secretion are as follows: ~1000 μg/ml for the 17.6 clone, ~135 μg/ml for the 17.4 clone and ~1 μg/ml for the 17.5 clone. The ratios of these allow us to estimate $k_m/k_e \approx 10$. While the absolute value of either of these is unknown, our rescaling of the equations bypasses the problem by considering only the ratio k_m/k_e.

For the model that includes APCs we must estimate $\bar{\alpha}_i \approx \alpha_i/A_d$, for $i = m, e$. It has been stated in Chu and Lowell (2005) that the steady state value of an antigen specific dendritic cells (DCs) is roughly $A_d = 4 \times 10^5$cells. Thus $\bar{\alpha}_m \approx [2.5-5] \times 10^{-5}$ and $\bar{\alpha}_e \approx [1.25-2.5] \times 10^{-5}(\text{cell day})^{-1}$. According to Kamath et al. (2000, 2002), the half life of APCs (DCs) is $\approx [1.5-2.9]$ days. Hence their turnover rate is $\delta_a \approx \ln(2)/[1.5-2.9] = [0.24-0.46]\text{day}^{-1}$. For $k_a = 0$ in Eq. (16), the solution for $A(t)$ is

$$A(t) = \frac{\sigma_a - \mathcal{K}\exp(-\delta_a t)}{\delta_a}$$

From data in Chu and Lowell (2005), $A(4) = 3 \times 10^5$ and $A(6) = 5 \times 10^5$ (time in days), we deduce that $\sigma_a \approx [3-4] \times 10^5$ cell/day and $\mathcal{K} = [5-14] \times 10^5$. Since $A_d \approx 4 \times 10^5$ cells, we conclude that

$$A_d = \frac{\sigma_a}{\delta_a + k_a M_d} \quad \Longrightarrow \quad k_a \approx [8-9] \times 10^{-6}(\text{cell day})^{-1}$$

For β cell parameters, we used Teta et al. (2005), Magami et al. (2002) and Kulkarni (2004), to estimate $d \approx [0.001-0.007]$. Bock et al. (2003), estimated that the total islet volume in mice is around 2 mm^3 of which β cells occupy 65–80% (see also Marée et al. (2006a)). Thus the range of β cell population in healthy mice at steady state is approximately $B_h \approx 4 \times 10^5 \times 2 \times [0.65-0.8] \approx [5-6] \times 10^5$cells, which is consistent with the range of values obtained in Jo et al. (2007). There are no available experimental data to determine the value of s (Bonner-Weir, 2001) and k_B. However, Fig. 10(b) suggests that $s \approx [560-1000]$ cells/day and $k_B \approx [7.5-11] \times 10^3$ cells. (It follows that the replication rate $r \approx s/(k_B + B_d)$ is roughly $[0.008-0.015]$ cell^{-1} which is consistent with the estimate in Dor et al. (2004).) We have used the same technique to estimate $\bar{R} \approx [2.7-3.2] \times 10^{-4}$ peptide-units/cell. Finally, it has been suggested that β cells are killed at a rate of

4300 cells/day (Kurrer et al., 1997). Therefore

$$\frac{\kappa E_d B_h}{1+\mu_0 B_h+\mu_1 M_d}=4300 \implies \frac{\kappa}{1+[5-6]\times 10^5\mu_0+0.5\times 10^5\mu_1} = \frac{4300}{[5-6]\times 10^{11}}\approx [7-8]\times 10^{-9}$$

According to Mahaffy and Edelstein-Keshet (2007), $\kappa \approx 0.14 \times 10^{-6}$ (cell day)$^{-1}$. Therefore we expect $\mu_0 \approx [1.67-20]\times 10^{-6}$ cell^{-}1 and $\mu_1 \approx [1.1-3.6]\times 10^{-4}$ cell^{-1}.

References

Anderson, B., Park, B.J., Verdaguer, J., Amrani, A., Santamaria, P., 1999. Prevalent CD8+ T cell response against one peptide/MHC complex in autoimmune diabetes. Proc. Natl. Acad. Sci. USA 96, 9311–9316.

Bock, T., Pakkenberg, B., Buschard, K., 2003. Increased islet volume but unchanged islet number in ob/ob mice. Diabetes 52, 1716–1722.

Bonner-Weir, S., 2001. β-cell turnover: its assessment and implication. Diabetes 50 (1), S20–S24.

Chu, C.L., Lowell, C.A., 2005. The lyn tyrosine kinase differentially regulates dendritic cell generation and maturation. J. Immunol. 175, 2880–2889.

De Boer, R.J., Perelson, A.S., 1994. T Cell repertoires and competitive exclusion. J. Theor. Biol. 169, 375–390.

Dor, Y., Brown, J., Martinez, O.I., Melton, D.A., 2004. Adult pancreatic beta-cells are formed by self-duplication rather than stem cell differentiation. Nature 429, 41–46.

Finegood, D.T., Scaglia, L., Bonner-Weir, S., 1995. Dynamics of β-cell mass in the growing rat pancreas. Estimation with a simple mathematical model. Diabetes 44, 249–256.

Han, B., Serra, P., Amrani, A., Yamanouchi, J., Marée, A.F.M., Edelstein-Keshet, L., Santamaria, P., 2005a. Prevention of diabetes by manipulation of anti-IGRP autoimmunity: high efficiency of a low-affinity peptide. Nature Med. 11, 645–652.

Han, B., Serra, P., Yamanouchi, J., Amrani, A., Elliott, J.F., Dickie, P., DiLorenzo, T.P., Santamaria, P., 2005b. Developmental control of CD8+ T cell-avidity maturation in autoimmune diabetes. J. Clin. Invest. 115, 1879–1887.

Jo, J., Choi, M.Y., Koh, D.S., 2007. Size distribution of mouse Langerhans islets. Biophys. J. 93, 2655–2666.

Kamath, A.T., Pooley, J., O'Keeffe, M.A., Vremec, D., Zhan, Y., Lew, A.M., Amico, A.D., Wu, L., Tough, D.F., Shortman, K., 2000. The development, maturation, and turnover rate of mouse spleen dendritic cell populations. J. Immunol. 165, 6762–6770.

Kamath, A.T., Henri, S., Battye, F., Tough, D.F., Shortman, K., 2002. Developmental kinetics and life span of dendritic cells in mouse lymphoid organs. Blood 100, 1734–1741.

Kulkarni, R.N., 2004. Cells in focus: The islet β-cell. Int. J. Biochem. Cell Biol. 36, 365–371.

Kurrer, M.O., Pakala, S.V., Hanson, H.L., Katz, J.D., 1997. β cell apoptosis in T cell-mediated autoimmune diabetes. Proc. Natl. Acad. Sci. USA 94, 213–218.

Lieberman, S.M., Evans, A.M., Han, B., Takaki, T., Vinnitskaya, Y., Caldwell, J.A., Serreze, D.V., Shabanowitz, J., Hunt, D.F., Nathenson, S.G., Santamaria, P., DiLorenzo, T.P., 2003. Identification of the β cell antigen targeted by a prevalent population of pathogenic CD8+ T cells in autoimmune diabetes. Proc. Natl. Acad. Sci. USA 100, 8384–8388.

Lieberman, S.M., Takaki, T., Han, B., Santamaria, P., Serreze, D.V., DiLorenzo, T.P., 2004. Individual nonobese diabetic mice exhibit unique patterns of CD8 + T cell reactivity to three islet antigens, including the newly identified widely expressed dystrophia myotonica kinase. J. Immunol. 173, 6727–6734.

Magami, Y., Azuma, T., Inokuchi, H., Moriyasu, F., Kawai, K., Hattori, T., 2002. Heterogeneous cell renewal of pancreas in mice: [3H]-thymidine autoradiographic investigation. Pancreas 24, 153–160.

Mahaffy, J.M., Edelstein-Keshet, L., 2007. Modeling cyclic waves of circulating T-cells in autoimmune diabetes. SIAM J. Appl. Math. 67, 915–937.

Marée, A.F.M., Komba, M., Dyck, C., Labecki, M., Finegood, D.T., Edelstein-Keshet, L., 2005. Quantifying macrophage defects in type 1 diabetes. J. Theor. Biol. 233, 533–551.

Marée, A.F.M., Kublik, R., Finegood, D.T., Edelstein-Keshet, L., 2006a. Modelling the onset of Type 1 Diabetes: can impaired macrophage phagocytosis make the difference between health and disease? Phil. Trans. Royal Soc. London (Series A) 364, 1267–1282.

Marée, A.F.M., Santamaria, P., Edelstein-Keshet, L., 2006b. Modeling competition among autoreactive CD8$^+$ T cells in autoimmune diabetes: implications for antigen-specific therapy. Int. Immunol. 18, 1067–1077.

O'Brien, B.A., Fieldus, W.E., Field, C.J., Finegood, D.T., 2002a. Clearance of apoptotic beta-cells is reduced in neonatal autoimmune diabetes-prone rats. Cell Death. Differ. 9, 457–464.

O'Brien, B.A., Huang, Y., Geng, X., Dutz, J.P., Finegood, D.T., 2002b. Phagocytosis of apoptotic cells by macrophages from NOD mice is reduced. Diabetes 51, 2481–2488.

Sallusto, F., Lanzavecchia, A., 2001. Exploring pathways for memory T cell generation. J. Clin. Invest. 108, 805–806.

Sherry, N.A., Kushner, J.A., Glandt, M., Kitamura, T., Brillantes, A.M.B., Herold, K.C., 2006. Effects of autoimmunity and immune therapy on β-cell turnover in type 1 diabetes. Diabetes 55, 3238–3245.

Shochat, E., Kedar, V., Segel, L.A., 2007. G-CSF control of neutrophils dynamics in the blood. Bull. Math. Biol. 69, 2299–2338.

Sreenan, S., Pick, A.J., Levisetti, M., Baldwin, A.C., Pugh, W., Polonsky, K.S., 1999. Increased β-cell proliferation and reduced mass before diabetes onset in the nonobese diabetic mouse. Diabetes 48, 989–996.

Teta, M., Long, S.Y., Wartschow, L.M., Rankin, M.M., Kushner, J.A., 2005. Very slow turnover of β-cells in aged adult mice. Diabetes 54, 2557–2567.

Thyssen, S., Arany, E., Hill, D.J., 2006. Ontogeny of regeneration of beta-cells in the neonatal rat after treatment with Streptozotocin. Endocrinology 147, 2346–2356.

Trudeau, J.D., Kelly-Smith, C., Verchere, C.B., Elliott, J.F., Dutz, J.P., Finegood, D.T., Santamaria, P., Tan, R., 2003. Prediction of spontaneous autoimmune diabetes in NOD mice by quantification of autoreactive T cells in peripheral blood. J. Clin. Invest. 111, 217–223.

Tsai, S., Shameli, A., Serra, P., Yamanouchi J., Medarova Z., Moore A., Santamaria, P., 2008. Reversal of autoimmunity by boosting autoregulatory T-cell memory. Submitted to Nature.

Veiga-Fernandes, H., Walter, U., Bourgeois, C., McLean, A., Rocha, B., 2000. Response of naive and memory CD8+ T cells to antigen stimulation in vivo. Nat. Immunol. 1, 47–53.

Viola, A., Lanzavecchia, A., 1996. T Cell Activation Determined by T Cell Receptor Number and Tunable Thresholds. Science 273, 104–106.

von Herrath, M., Sanda, S., Herold, K., 2007. Type 1 diabetes as a relapsing-remitting disease? Nature Rev. Immunol. 7, 988–994.